AD-A269 978

‖‖‖‖‖‖‖‖‖‖‖‖‖‖‖‖

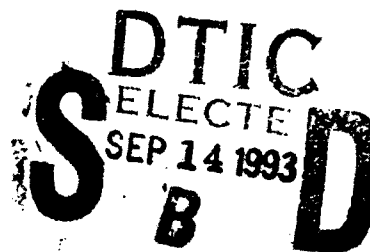# REMOTE SOUNDING OF TEMPERATURES IN CLOUDY ATMOSPHERES USING THE DIFFERENTIAL INVERSION METHOD

S. C. Ou
K. N. Liou

University of Utah
Center for Atmospheric and
Remote Sounding Studies (CARSS)
Department of Meteorology
Salt Lake City, Utah 84112

DTIC
ELECTE
SEP 14 1993
S B D

28 February 1992

Final Report
1 October 1989-31 December 1991

PHILLIPS LABORATORY
Directorate of Geophysics
AIR FORCE SYSTEMS COMMAND
HANSCOM AFB, MA 01731-5000

93-21411
‖‖‖‖‖‖‖‖‖‖‖‖‖‖‖

"This technical report has been reviewed and is approved for publication"

Jean A. Kuria

Contract Manager

Robert A. McClatchey

Division Director

This report has been reviewed by the ESC Public Affairs Office (PA) and is releasable to the National Technical Information Service (NTIS).

Qualified requestors may obtain additional copies from the Defense Technical Information Center. All others should apply to the National Technical Information Service.

If your address has changed, or if you wish to be removed from the mailing list, or if the addressee is no longer employed by your organization, please notify PL/TSI, Hanscom AFB, MA 01731-5000. This will assist us in maintaining a current mailing list.

Do not return copies of this report unless contractual obligations or notices on a specific document requires that it be returned.

REPORT DOCUMENTATION PAGE

Public reporting burden for this collection of information is estimated to average 1 hour per response, including the time for reviewing instructions, searching existing data sources, gathering and maintaining the data needed, and completing and reviewing the collection of information. Send comments regarding this burden estimate or any other aspect of this collection of information, including suggestions for reducing this burden, to Washington Headquarters Services, Directorate for information Operations and Reports, 1215 Jefferson Davis Highway, Suite 1204, Arlington, VA 22202-4302, and to the Office of Management and Budget, Paperwork Reduction Project (0704-0188), Washington, DC 20503.

1. AGENCY USE ONLY (Leave blank)	2. REPORT DATE 28 February 1992	3. REPORT TYPE AND DATES COVERED Final (1 Oct 1989 – 31 Dec 1991)

4. TITLE AND SUBTITLE	5. FUNDING NUMBERS
Remote Sounding of Temperature in Cloudy Atmospheres Using the Differential Inversion Method	PE 61102F PR 2310 TA G8 WU AH
6. AUTHOR(S) S. C. Ou K. N. Liou	Contract F19628-90-K-0004

7. PERFORMING ORGANIZATION NAME(S) AND ADDRESS(ES)	8. PERFORMING ORGANIZATION REPORT NUMBER
University of Utah Ctr for Atmospheric & Remote Sounding Studies (CARSS) Department of Meteorology Salt Lake City, Utah 84112	

9. SPONSORING/MONITORING AGENCY NAME(S) AND ADDRESS(ES)	10. SPONSORING/MONITORING AGENCY REPORT NUMBER
Phillips Laboratory Hanscom AFB, MA 01731-5000 Contract Manager: Jean King/GPA	PL-TR-92-2337

11. SUPPLEMENTARY NOTES

12a. DISTRIBUTION/AVAILABILITY STATEMENT	12b. DISTRIBUTION CODE
Approved for public release; Distribution unlimited	

13. ABSTRACT (Maximum 200 words)

We have assessed the applicability of the Differential Inversion (DI) method to temperature retrievals in both clear and cloudy atmospheres using real satellite data. The main theme of the DI is that the local Planck intensity can be exactly expressed by a linear combination of the derivatives of radiances in the logarithmic pressure coordinate. The satellite data set used in this work contains collocated brightness temperatures and radiosonde data which have been collected during the period of BUAN experiments. A multi-spectral cloud-removal method using the principle of the N^*-method has also been developed. Retrieval results are presented in terms of rms temperature differences between retrieved and sounding profiles. Considering all clear and partly-cloudy cases, the rms differences in temperature of ~2 K for retrievals using the DI are comparable to those using the BUAN scheme. The rms differences in temperature for retrievals using the multi-spectral cloud removal scheme are slightly larger than those using the BUAN cloud-removal scheme by ~0.5 K. Finally, the rms temperature differences are much smaller than those for the BUAN first-guess.

14. SUBJECT TERMS		15. NUMBER OF PAGES
Remote sensing Linear inversion theory Cloud-removal method	Differential inversion method HIRS Temperature retrieval	68
		16. PRICE CODE

17. SECURITY CLASSIFICATION OF REPORT	18. SECURITY CLASSIFICATION OF THIS PAGE	19. SECURITY CLASSIFICATION OF ABSTRACT	20. LIMITATION OF ABSTRACT
Unclassified	Unclassified	Unclassified	SAR

TABLE OF CONTENTS

Accession For

NTIS   GRA&I

DTIC TAB

Unannounced

Justification

By

Distribution/

Availability Codes

Avail and/or

Special

Dist

A-1

Section 1

INTRODUCTION

Although operational retrievals of temperature profiles have been routinely performed in the past 15 years, the techniques and procedures used have been under constant refinement. This is because the retrieval of atmospheric temperature profiles is a complicated problem in which consistent and accurate performance is difficult to achieve. Many retrieval methods have been proposed in the past; these can be categorized into two groups: statistical and physical methods.

Statistical methods determine temperature profiles based on results from regression analyses of collocated satellite and sounding data. While statistical methods are computationally fast, the accuracy of the retrieval temperatures varies significantly. Physical methods determine temperature profiles by solving an ill-conditioned and ill-posed Fredholm integral equation of the first kind. Because of the unstable characteristics of the solution process, conventional physical methods prescribe first-guess profiles (for reference) and specify external constraints to control the behavior of the solution. For example, the minimum variance scheme (Fleming et al., 1986; Eyre, 1989) utilizes numerical weather prediction models or statistical library search procedures to generate first-guesses and the use of elements of error covariance matrices to control the smoothness of the resulting temperature profiles.

Current efforts focus on the search for better first-guess profiles. Recently, McMillin (1991) employed a classification method to obtain reasonable first-guess temperature profiles, but improvement of the retrieval accuracies was nominal (~0.2-0.3 K, rms). Other efforts have also produced inconclusive results. In the BUAN (Baseline Upper Atmospheric Network) experiment, it was

1

theorized that better collocation would lead to better retrievals. For this reason, the size of temporal and spatial collocation windows were reduced from ±3 hour and ±300 km to ±1 hour and ±150 km, but no significant retrieval improvements were achieved (Bloom and Nappi, 1990).

It has been suggested that increasing the number of sensing channels may yield additional information content for temperature retrievals and improve retrieval accuracy. Along this line, simulation studies based on the Advanced Moisture and Temperature Sounders (AMTS) showed that better retrievals can be achieved by using high resolution channels (Phillips et al., 1988). Smith et al (1990) demonstrated that root-mean-square temperature errors can be reduced to 1-1.5 K by using hundreds of channels on the High Resolution Interferometer Sounder (HIS) while onboard aircraft, but only limited cases for a short time interval and over a small geographical locality have been tested.

In an attempt to circumvent conventional techniques, King (1985) proposed a novel linear transform approach to solve the temperature retrieval problem. This approach is referred to as the differential inversion method (DI). The essence of the DI is that, based on the convolution theory, the Laplace transform of Planck intensity profile is linearly related to the Laplace transform of radiance profile. By applying the inverse transform, the local Planck intensity can be expressed as a linear combination of the derivatives of radiances in the logarithmic peak pressure coordinate. Instead of using external constraints to "regularize" the retrieved temperature profile, it is assumed that the radiances can be represented by smooth polynomial functions, so that the derivatives of radiances can be computed. Thus the DI offers an alternative approach for solving the temperature retrieval problem in that prescription of the first-guess profile and the associated error covariance matrices are not required.

Many theoretical aspects of the DI have been explored (Liou and Ou, 1988; Liou et al., 1989; Ou and Liou, 1989). It has been shown that the DI is efficient, stable, and particularly practical for narrow weighting functions. The purpose of this work is to further examine the applicability of DI to temperature retrievals. Fundamentals of the DI are presented in Section 2.

We have acquired the BUAN data set to test whether the DI can be applied to the retrieval of atmospheric temperature profiles using satellite data. This data set contains a large number of collocated satellite and radiosonde observations which were collected between January 15 and July 15, 1988. It also includes results of temperature retrievals using the operational method for both clear and partly cloudy conditions. We have used the data set for the following purposes: (1) to perform simulation studies for the development of a multi-channel cloud-removal method, (2) to develop an adjustment scheme for measured radiances, and (3) to compare retrieval results using the DI operational methods. Details of the BUAN data set and the transmittance model for radiative transfer calculations are given in Section 3.

To apply the DI to retrieving temperature profiles in partly cloudy atmospheres, clear radiances must be reconstructed from cloud contaminated radiances. Many cloud-removal methods have been proposed in conjunction with various retrieval schemes. Eyre and Watts (1987) have reviewed cloud-removal methods which have been developed up to 1987. Most of these methods follow the principles of the N^*-method proposed by Smith (1968). The quantity N^* is the ratio of effective cloud covers for adjacent pixels and is the basic parameter used to reconstruct clear radiances. Different approaches have also been used to determine N^*, which are basically statistical in nature. For example, Smith and Woolf (1976) combined HIRS and SCAMS data from Nimbus 6 to determine N^* and clear radiances simultaneously using the eigenvectors of the covariance matrix

3

of clear radiances. McMillin and Dean (1982) employed radiances of both HIRS 4.3 μm channels and MSU (microwave) channels to compute N^* using an interchannel regression technique. We have developed a new approach that uses the HIRS Chs. 6, 7, and 8 radiances to simultaneously determine surface temperature, clear radiances and N^* based on results from radiative transfer simulations. The method solves two sets of equations by iteration. One set is the multispectral correlations of the simulated clear radiances while the other is the linear relationships between the partly cloudy radiances over adjacent pixels. Details of the cloud removal method are provided in Section 4.

While the DI is a linear inversion method, the problem involving atmospheric temperature retrievals using satellite data is highly nonlinear. To apply the DI for temperature retrievals using either original or cloud-removed clear radiances, these radiances must be adjusted so that major nonlinear components are removed. For the minimum-variance method, adjustment processes are implicitly included in the specification of the first guesses, the error covariance matrices and the kernel matrix characterizing forward radiative transfer. In the present work, adjustment takes the form of correlation between simulated and linear radiances. Discussion of the adjustment of radiances is given in Section 5. Retrieval results and discussions are presented in Section 6. Finally, conclusions are presented in the final Section.

Section 2

FUNDAMENTALS OF THE

DIFFERENTIAL INVERSION METHOD

2.1 Forward Radiative Transfer Equation

The upwelling radiance at the top of the atmosphere, R_ν, for a given spectral band may be derived from the solution of the basic radiative transfer equation. Assuming a plane-parallel atmosphere under local thermodynamic equilibrium, we have

$$R_\nu = B_\nu(T_s) \, T_\nu(p_s) + \int_{p_s}^{0} B_\nu(p) \, \frac{\partial T_\nu(p)}{\partial p} \, dp, \qquad (2.1)$$

where B_ν is the Planck intensity at central wave number ν, T_ν is the transmittance, p_s is the surface pressure, and T_s is the surface temperature. The first and second terms represent surface and atmospheric emission contributions, respectively.

The slab below the surface may be viewed as a semi-infinite isothermal emitter whose temperature is T_s, and whose pressure increases from p_s downward to ∞. For $p \to \infty$, $T_\nu(\infty)$ is taken to be 0. Thus $T_\nu(p_s)$ can be expressed by the following mathematical identity:

$$T_\nu(p_s) = T_\nu(p_s) - T_\nu(\infty) = \int_{\infty}^{p_s} \frac{\partial T_\nu(p)}{\partial p} \, dp. \qquad (2.2)$$

Multiplying both sides of Eq. (2.2) by $B_\nu(T_s)$, we obtain

$$B_\nu(T_s) \, T_\nu(p_s) = \int_{\infty}^{p_s} B_\nu(p_s) \, \frac{\partial T_\nu(p)}{\partial p} \, dp. \qquad (2.3)$$

Combining Eqs. (2.1) and (2.3) leads to the following forward radiative transfer equation in continuous form:

$$R_{\nu} = \int_{p_{s}}^{0} B_{\nu}(p) \; \frac{\partial T_{\nu}(p)}{\partial p} \; dp, \tag{2.4}$$

where $B_{\nu}(p) = B_{\nu}(T_{s})$ for $p_{s} < p < \infty$.

We next define the weighting function as follows:

$$W_{\nu}(p) = - p \; \frac{\partial T_{\nu}(p)}{\partial p}. \tag{2.5}$$

The weighting function controls the relative contribution of atmospheric emission from various levels. Because $T_{\nu}(p)$ decreases as p increases, $\partial T_{\nu}(p)/\partial p < 0$, but $W_{\nu}(p) > 0$ for $0 < p < \infty$. Quantitatively, $\partial T_{\nu}(p)/\partial p$ depends on the vertical distribution of absorbing gases and temperature. Near the top of the atmosphere, $T_{\nu}(p)$ decreases slowly downward due to the low density of absorbing gases. As the density of absorbing gases increases with p, the rate of decrease in $T_{\nu}(p)$ increases. Finally, as p approaches p_{s}, $T_{\nu}(p)$ approaches 0, and $\partial T_{\nu}(p)/\partial p$ also approaches 0. Thus, a maximum value of $|\partial T_{\nu}(p)/\partial p|$ or W_{ν} must exist between the top of the atmosphere and the surface, signifying the maximum rate of change of $T_{\nu}(p)$. Let the pressure level corresponding to maximum W_{ν} be $\bar{p}$, this value varies with the concentration of absorbing gases, temperature, and wave number ν. If the wave number of a channel is near the band center, $T_{\nu}(p)$ decreases rapidly downward due to strong absorption, so that $\bar{p}$ is located at a relatively high altitude. If the wave number is near the band wing, the atmosphere will be relatively transparent and $T_{\nu}(p)$ does not vanish at $p = p_{s}$, so that $\bar{p}$ will be near the surface.

2.2 Differential Inversion Method

We shall approach the inverse problem by a transformation of variables. The following variables are introduced: $\bar{\xi} = -\ell n \bar{p}$ and $\xi = -\ell n p$, where $\bar{p}$ is the

peak pressure of the weighting function W. In terms of these new variables, Eq. (2.4) can be rewritten as (King, 1985; Liou and Ou, 1988)

$$R(\bar{\xi}) = \int_{-\infty}^{\infty} B(\xi) \, W(\xi - \bar{\xi}) d\xi, \qquad (2.6)$$

where $R(\bar{\xi}) = R_\nu(\bar{p})$, $B(\xi) = B_\nu(p)$, and $W(\xi - \bar{\xi}) = W(p,\bar{p})$. Assume that R is some smooth function of the variable $\bar{\xi}$, for which higher-order derivatives exist. This assumption implies that for each value of $\bar{\xi}$, there is a corresponding weighting function $W(\xi - \bar{\xi})$. Subsequently, we perform a bilateral Laplace transform (Widder, 1971) on both sides of Eq. (2.6), and use the convolution theory to obtain

$$r(s) = b(s)w(-s), \qquad (2.7)$$

where s denotes the transform variable, and $r(s)$, $b(s)$ and $w(-s)$ represent the bilateral Laplace transforms of R, B, and W, respectively. Based on Eq. (2.7), we can obtain $B(\bar{\xi})$ as follows:

$$B(\bar{\xi}) = L^{-1} \left[\frac{r(s)}{w(-s)} \right], \qquad (2.8)$$

where L^{-1} is the inverse bilateral Laplace transform. The term $1/w(-s)$ may be expanded into a MacLaurin series (Pearson, 1971) so that

$$\frac{1}{w(-s)} = \sum_{n=0}^{\infty} \lambda_n s^n, \qquad (2.9)$$

where the coefficient λ_n is related to the nth derivative of the function $1/w(-s)$ evaluated at $s = 0$ as follows:

$$\lambda_n = \left[\frac{1}{w(-s)} \right]_{s=0}^{(n)} / n! . \qquad (2.10)$$

By inserting Eq. (2.9) into Eq. (2.8), and noting that λ_n's are constants, we have

7

$$B(\bar{\xi}) = \sum_{n=0}^{\infty} \lambda_n L^{-1} \left[s^n r(s) \right]. \tag{2.11}$$

We may use expressions for the Laplace transform of the nth derivative of the function $R(\bar{\xi})$ to determine the inverse transform of $s^n r(s)$. Using this procedure, $B(\bar{\xi})$ can be expressed in terms of a linear sum of radiance derivatives at $\bar{\xi}$ as follows:

$$B(\bar{\xi}) = \sum_{n=0}^{\infty} \lambda_n \frac{d^n R(\bar{\xi})}{d\bar{\xi}^n} . \tag{2.12}$$

In order to evaluate higher derivatives on the right side of Eq. (2.12), $R(\bar{\xi})$ must be a smooth function of $\bar{\xi}$. In principle, the solution of $B(\bar{\xi})$ would be mathematically exact for infinite summations. However, for narrow weighting functions, λ_n converges rapidly to zero, so that the summation of Eq. (2.12) may be truncated to just a few terms.

2.3 Weighting Functions and Inversion Coefficients

The determination of $B(\bar{\xi})$ from Eq. (2.12) requires knowledge of both λ_n and the derivatives of $R(\bar{\xi})$. The inversion coefficient λ_n depends on the weighting function W. The bilateral Laplace transform of W can be expressed by

$$w(-s) = \int_0^{\infty} \tilde{p}^{-s} W(\tilde{p}) \, d\tilde{p}/\tilde{p}, \tag{2.13}$$

where $\tilde{p} = p/\bar{p}$. In principle, if the atmospheric temperature and humidity profiles are known, it is then possible to evaluate w, and subsequently $1/w(-s)$ and its derivatives numerically through accurate line-by-line spectral integrations. However, because atmospheric parameters are not known before retrieval, the above numerical approach is not practical, and we prefer to develop an analytic form that can adequately approximate the weighting functions. A generalized weighting function has been proposed by King (1985) in the form

8

$$W_\kappa(\bar{p}) = \kappa^{(\kappa-1/\kappa)} \Gamma^{-1}(1/\kappa) \bar{p} \exp(-\bar{p}^\kappa/\kappa),$$ (2.14)

where Γ is the Gamma function and κ is an index controlling the sharpness of the weighting function. Figure 1 shows the functional form of W_κ for $\kappa = 0.5$, 1, and 2. Smaller values of κ correspond to broader weighting functions with lower peak values. The range of significant contribution of the weighting function is from $\bar{p} = 0.1$ to $\bar{p} = 10$, spanning two orders of magnitude.

Using the functional form of Eq. (2.14), we can show that

$$w(-s) = \Gamma[(1-s)/\kappa)]/[\Gamma(1/\kappa)\kappa^{s/\kappa}] .$$ (2.15)

Evaluation of $w(-s)$, and therefore of λ_n, based on Eqs. (2.13) and (2.10) involves digamma and polygamma functions (Abramowitz and Stegun, 1972). Expressions for λ_n as functions of κ have been given by King (1985) for $n=1$ to 5. Figure 2 shows the inversion coefficients λ_n for $n=1$ to 5 as functions of κ. For $\kappa > 1$, $-1 < \lambda_n < 0.2$, and λ_n decreases in magnitude as κ increases. In addition, based on Eq. (2.12), any error inherent in the derivatives of $R(\bar{\xi})$ would be substantially suppressed in the retrieved $B(\bar{\xi})$, because λ's converge to zero for larger n. For $\kappa < 1$, $|\lambda_1|$, $|\lambda_3|$, and $|\lambda_5|$ are still less than 1, but $|\lambda_2|$ and $|\lambda_4|$ increase sharply with decreasing κ. Errors in radiances will then be amplified through λ_2 and λ_4 and propagate into the computation of $B(\bar{\xi})$.

2.4 Polynomial Fitting of Radiance Profiles

Evaluation of higher derivatives of $R(\bar{\xi})$ is based on the assumption that radiances can be represented by smooth functions in terms of the variable $\bar{\xi}$. We propose to express $R(\bar{\xi})$ in terms of an (N-1)th degree polynomial of $\bar{\xi}$ in the form

$$R(\bar{\xi}) = \sum_{m=0}^{N-1} a_m \bar{\xi}^m.$$ (2.16)

Substituting Eq. (2.16) into Eq. (2.12) leads to

9
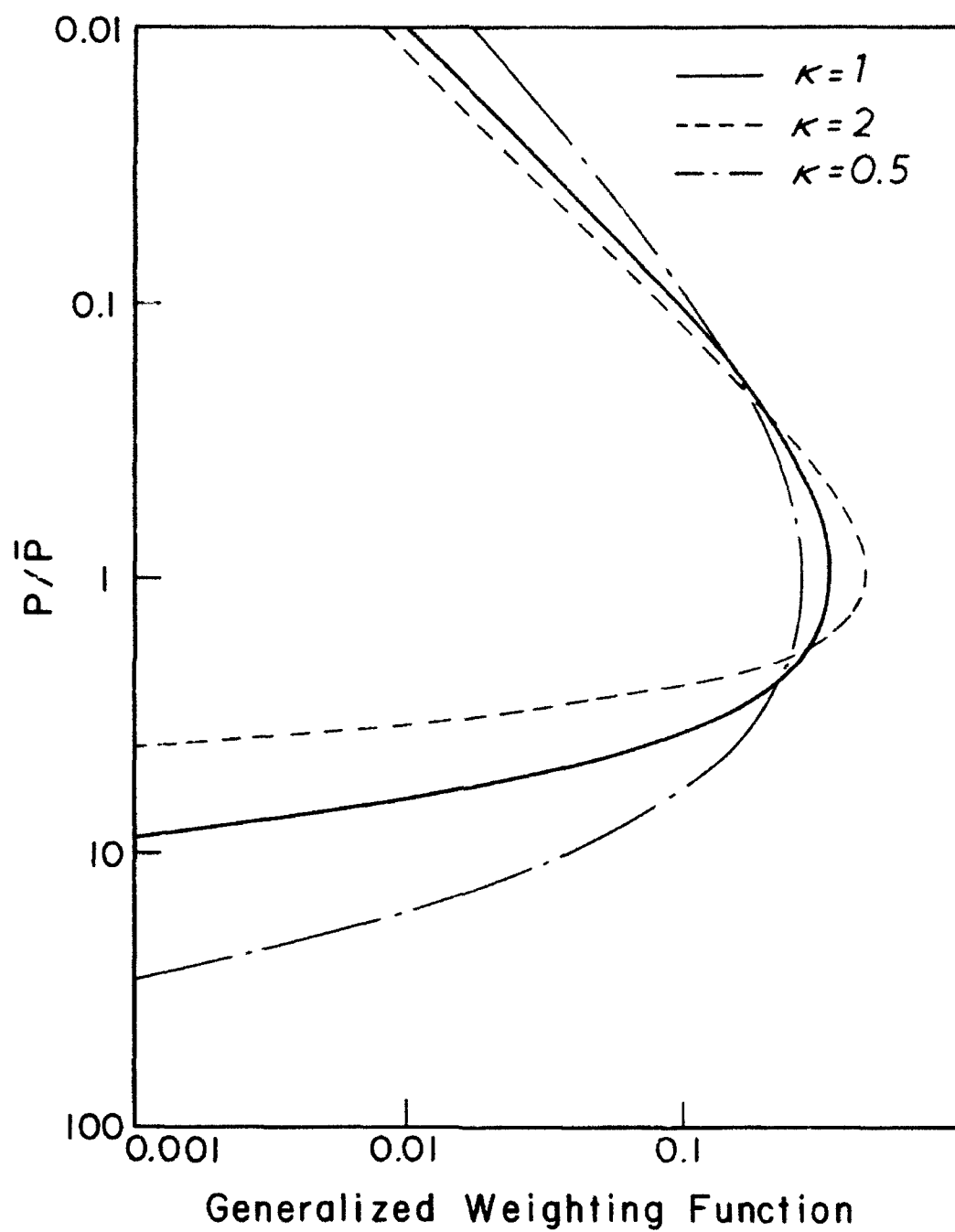
Fig. 1   The generalized weighting function as a function of p/p̄ for the
           sharpness index κ – 0.5, 1, and 2.

10
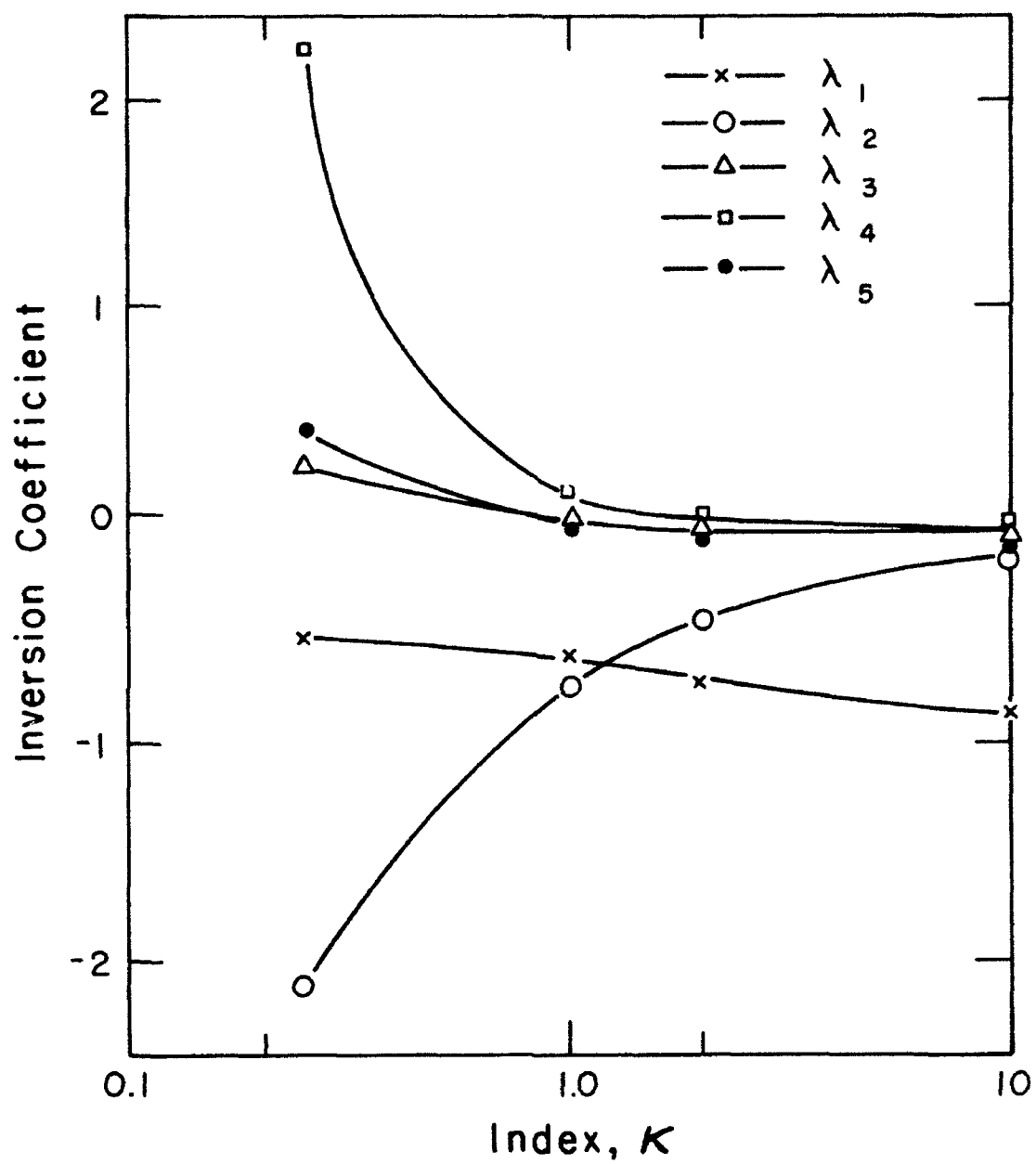
Fig. 2   Inversion coefficients λ_i (i = 1.-5) as functions of the index κ.

11

$$B(\overline{\xi}) = \sum_{n=0}^{N-1} \lambda_n \sum_{m=n}^{N-1} \frac{m! \, a_m}{(m-n)!} \, \overline{\xi}^{m-n}. \tag{2.17}$$

Equation (2.17) is also an (N-1)th degree polynomial. In practice, there are only a finite number of radiances that correspond to a finite number of $\overline{\xi}_i$. The unknown polynomial coefficients in Eq. (2.16) can be obtained by least-square fitting of the finite number of $R(\overline{\xi}_i)$ to a polynomial. Since errors in the fitting radiances at $\overline{\xi}_i$ are minimized, the first term of Eq. (2.12) at these $\overline{\xi}_i$ would be more reliable than at other $\overline{\xi}$ values between neighboring $\overline{\xi}_i$. Note that emission from regions near $\overline{p}_i$ makes the dominant contribution to upwelling radiances, and it would be physically meaningful to present results in terms of the temperatures at discrete $\overline{\xi}_i$ values.

Section 3

DATA SET USED IN TEMPERATURE RETRIEVAL STUDIES

We have acquired from NESDIS a large data set of collocated temperature profiles and satellite data. These data were collected during the observation period (Jan 15 - Jul 15, 1988) of the Baseline Upper Air Network (BUAN) experiment. Since primary goal of the experiment was to test the hypothesis that the accuracy of temperature retrieval can be improved if better collocation data are available, the BUAN data set represents the best collocated satellite data set so far available for temperature retrieval studies. We were also provided with the transmittance model currently being used in NESDIS which computes atmospheric transmittances due to the absorption by water vapor continuum and rotational bands, CO_2 15 μm band, ozone 9.6 μm band for the 19 HIRS channels.

3.1 BUAN Data Set

3.1.1 Satellite Data Set

The BUAN data set contains satellite data measured by the radiometers on board NOAA-10. The data of NOAA-9 were not available during the field experiment due to an instrument malfunction. NOAA-10 had local equator crossing times of approximately 0730 and 1930 LTC. Except in polar regions, satellite overpass generally coincides with the 0000 and 1200 UTC routine synoptic observations at about 100 E and 80 W and with the 0600 and 1800 UTC standard observations at about 30 E and 170 W.

There are two levels of data set. The level 1-T (match file B) contains original brightness temperature data for the 19 HIRS, four MSU and three SSU channels. These brightness temperature data have been converted from counts recorded by the radiometer for all weather conditions, including clear, partly

13

cloudy and overcast situations. Each record contains the sounder data over a "box" which consists of an array of 9x11 spots, as shown in Fig. 3. Only the data for the 9x7 spots within the solid frame of Fig. 1 have been used for retrieval analysis. One or more radiosonde stations are also located within the domain of the 9x7 spots ("+" in the diagram). The BUAN retrieval procedures have been documented by Reale et al. (1986). A brief description is provided in the Appendix.

The other level of data (match file A) contains the BUAN retrieval products. These include specifications of the spot for which retrievals are performed, the associated latitude,longitude, date, and time, the "raw" and cloud-removed clear radiances, the retrieved temperature and humidity profiles, the average value of N^* (used in the cloud-removal scheme), surface albedo, skin temperature, surface elevation, and first-guess temperature and humidity profiles. It is noted that the "raw" clear radiances are directly adopted from the brightness temperatures for an identified clear spot, and that the "cloud-removed" clear radiances are generated from the BUAN N^*-method.

3.1.2 Collocated Data Set of Radiosonde Observations

BUAN radiosonde and satellite observations were collocated and saved each day during the period of data collection. The general procedures were to collect pairs of radiosonde and satellite observations that were within 1 hour and 150 km of each other. [The normal operational collocation window is ±3 hours and ±300 km (Kalnay et al., 1990).] The radiosonde data contains vertical profiles of pressure, temperature, dew-point depression, geopotential height, wind direction and wind speed. These data were recorded in terms of 15 mandatory (all data) and 25 significant (temperature and pressure only) levels.

14
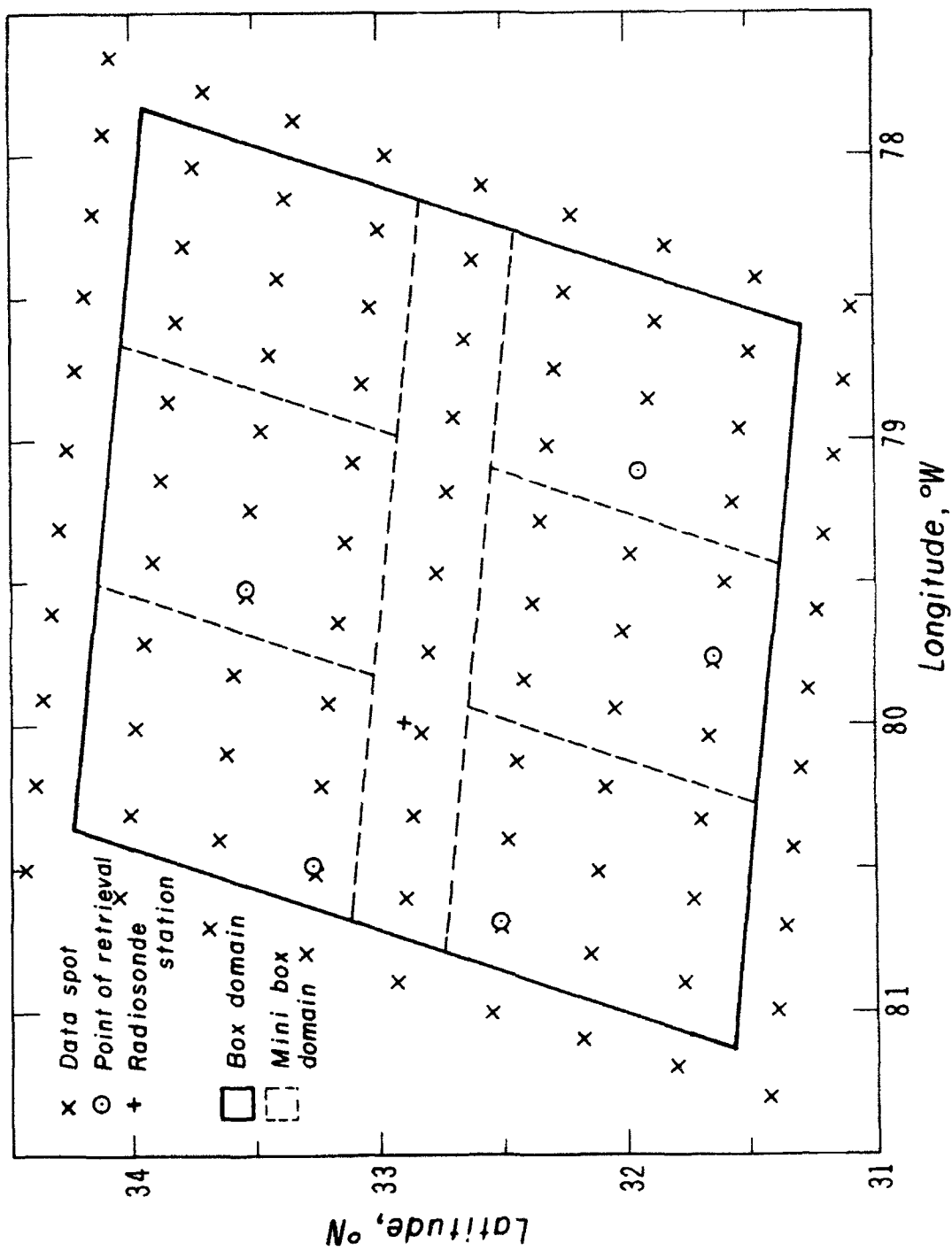
Fig. 3   Display of the array of 11x9 spots in a box. Each "x" denotes one spot. Cloud-clear analyses are performed for the 9x7 spots within the solid frame. These spots are further divided into six mini-boxes. Only one retrieval is done for each mini-box. The spot over which a retrieval is performed is denoted by "o." The rawinsonde station is denoted by "+." The distance between the station and the retrieval spot is less than 150 km.

3.2 Model for Computing Transmittances

The current operational transmittance model has been made available to us through NESDIS; it computes the vertical profiles of transmittances involving TOVS sounding channels. Spectral bands considered include water vapor continuum and rotational, O_3 - 9.3 μm, and CO_2 - 15 μm bands. For the water vapor continuum band, effects of pressure broadening due to N_2 and water vapor molecules are considered based on physical principles. For the rest of the absorption bands, parameterizations based on more detailed line-by-line computations were used (McMillin et al., 1979). To guarantee adequate match-up between the simulated and measured radiances, however, an adjustment factor γ was introduced. This factor varies with wave number and height. A single γ is used over all geographical locations, however. Without this factor, the simulated radiances will differ greatly from measurements (Fleming et al., 1986).

Section 4

CLOUD-REMOVAL METHOD

We have developed a method to restore clear radiances from cloud-contaminated brightness temperatures based on the principle of the N^*-method (Smith and Woolf, 1976), where the quantity N^* is the ratio of effective cloud covers over a pair of adjacent pixels. The current method differs from other N^*-methods in that N^* is determined using the radiances involving Chs. 6, 7 and 8 based on radiative transfer simulations. A detailed description of the current cloud-removal method is given below.

4.1 N^*-Method

For a pair of adjacent pixels, let the radiances for the ith channel over clear and cloudy areas be R_{oi} and R_{ci}, respectively. Then the radiances for pixels 1 and 2 are given by

$$R_{i1} = (1 - \eta_1) R_{oi1} + \eta_1 R_{ci1}, \tag{4.1a}$$

$$R_{i2} = (1 - \eta_2) R_{oi2} + \eta_2 R_{ci2}, \tag{4.1b}$$

where η_1 and η_2 are the effective cloud covers for the respective pixels. These effective covers are defined as the product of cloud cover and emissivity. We have assumed that over each of the adjacent pixels, only a single layer of cloud is present, and that clouds are located at the same altitude with the same cloud temperature. In addition, clouds are assumed to have the same radiative properties. This assumption is generally valid for water clouds which are thermally black. However, it cannot be applied to semi-transparent cirrus clouds, which are a subject currently under investigation. The above assumptions lead to the approximations $R_{oi1} - R_{oi2} - R_{oi}$ and $R_{ci1} - R_{ci2} - R_{ci}$. Consequently, we can eliminate R_{ci} from Eqs. (4.1a) and (4.1b) and obtain

17

$$N^* = \eta_1/\eta_2 = \frac{R_{oi} - R_{i1}}{R_{oi} - R_{i2}}. \qquad (4.2)$$

If we know N^* in advance, we may determine R_{oi} from Eq. (4.2) as follows:

$$R_{oi} = (R_{i1} - R_{i2}N^*)/(1 - N^*). \qquad (4.3)$$

The N^*-method is subject to the following restrictions:

1) The assumption that adjacent clouds are of the same height, temperature, and radiative properties may not be realistic. Clouds may occur at different heights with different temperature and radiative properties. In addition, multiple-layer clouds are often present. If the cloud properties for the adjacent pixels differ drastically, R_{oi} determined from Eq. (4.3) will be subject to large error, and therefore, in operational retrieval methods, efforts have been made to search for the pair of adjacent pixels that meet the assumption most closely (McMillin, 1978; McMillin and Dean, 1982).

2) To estimate N^* from Eq. (4.2), we must know the clear radiance of a channel which is not used in temperature retrieval. This implies that the surface temperature must be known. Over partly cloudy and overcast areas, observed IR and visible radiances are contaminated by clouds and cannot be directly used to determine surface temperature. An alternative approach is to use microwave channel radiance, but microwave measurements are usually subject to errors caused by poor resolution, contamination by precipitating clouds, and uncertainties in the estimated surface emissivity. The smallest pixel of MSU on board the NOAA polar-orbiting satellites has a diameter of about 110 km, which is more than six times larger than the diameter of HIRS pixels. In addition, since the wavelength of microwave channels is on the order of mm, the measured

microwave radiation is subject to scattering/absorption effects caused by precipitation drops with sizes larger than or comparable to the wavelength. Finally, the surface emissivity in the microwave region varies over a wide range. Over the oceans, the emissivity ranges from 0.45 to 0.65, depending on temperature and surface wind speed. Over land, the emissivity ranges from 0.90 to 0.95, depending on soil moisture. Over ice, the emissivity is usually > 0.7 (Burroughs, 1991). It is generally recognized that applying the microwave technique over land and ice is extremely difficult.

3) The N^*-method cannot be used when both pixels have the same amount of cloud cover. In this case, $N^*=1$ and the denominator in Eq. (4.3) becomes infinite.

4) The N^*-method will also fail when an inversion is present in the temperature profile. In this case, $R_{i1} \sim R_{i2} \sim R_{oi}$.

4.2 Multi-spectral Cloud Removal Scheme

We have developed a multi-spectral approach using the HIRS Chs. 6, 7 and 8 radiances to determine the surface temperature and clear radiances of these channels simultaneously. First, radiative transfer simulations are performed to develop correlations between clear radiances of the three channels, next the relationships are examined between partly-cloudy radiances of the same channels, and finally the algebraic equations are derived and solved based on the simulation analyses.

4.2.1 Multi-spectral Correlation of Clear Radiances

To economize the computational effort involving the calculation of clear radiances, the correlations of clear radiances have been developed for channels having peaks of the weighting function close to the surface. These correlations

are largely independent of temperature and humidity profiles. The BUAN sounding temperature and humidity profiles have been used to perform simulation studies. HIRS Chs. 6, 7, and 8 are selected because their weighting functions peak near the surface and they are sensitive to surface temperature and the presence of clouds. The correlations are developed in terms of $\Delta R_i = R_{si} - R_{oi}$, where R_{oi} and R_{si} are the clear radiance and surface emitted radiance for Ch. i.

Figures 4a and 4b show the correlations of ΔR_7 vs. ΔR_6 and ΔR_8 vs. ΔR_7, respectively. The quantities R_{o7} and R_{o6} are obtained based on radiative transfer simulations using a large number of temperature and humidity profiles contained in the BUAN data set. Weighting functions are computed using the NESDIS transmittance model. The correlation between Ch. 6 and Ch. 7 radiance difference is extremely good because the surface emission contributions have been removed. The ΔR_i values are dependent on the humidity. Small values would correspond to polar (dry) conditions, while large values would correspond to tropical (moist) conditions. For $\Delta R_6 > 40$ mW/m^2/sr/cm^{-1}, the computed points exhibit larger spread because of increasing humidity effects. The spread, however, is within only 3 mW/m^2/sr/cm^{-1}. The solid curve in Fig. 4 a is the quadrature fit in the form

$$\Delta R_7 = \sum_{n=0}^{2} d_n \, \Delta R_6^n, \qquad (4.4)$$

where $d_o = 0.5763$; $d_1 = 0.3736$; $d_2 = 0.0047$. The rms difference between simulated and fitted values of ΔR_7 is about 1 mW/m^2/sr/cm^{-1}. Thus, Eq. (4.4) is a reasonable representation of the correlation between Ch. 6 and Ch. 7 radiance differences. On the other hand, the correlation between Chs. 7 and 8 radiance differences, as shown in Fig. 4b in log-log plot, is less satisfactory. For $\Delta R_7 > 20$ mW/m^2/sr/cm^{-1}, its scatter decreases between 0.1 and 20 mW/m^2/sr/cm^{-1} as ΔR_7 increases. For $\Delta R_7 < 20$ mW/m^2/sr/cm^{-1}, although the computed data scatter widely, the ΔR_8 values < 2 mW/m^2/sr/cm^{-1}. Thus it is reasonable to approximate
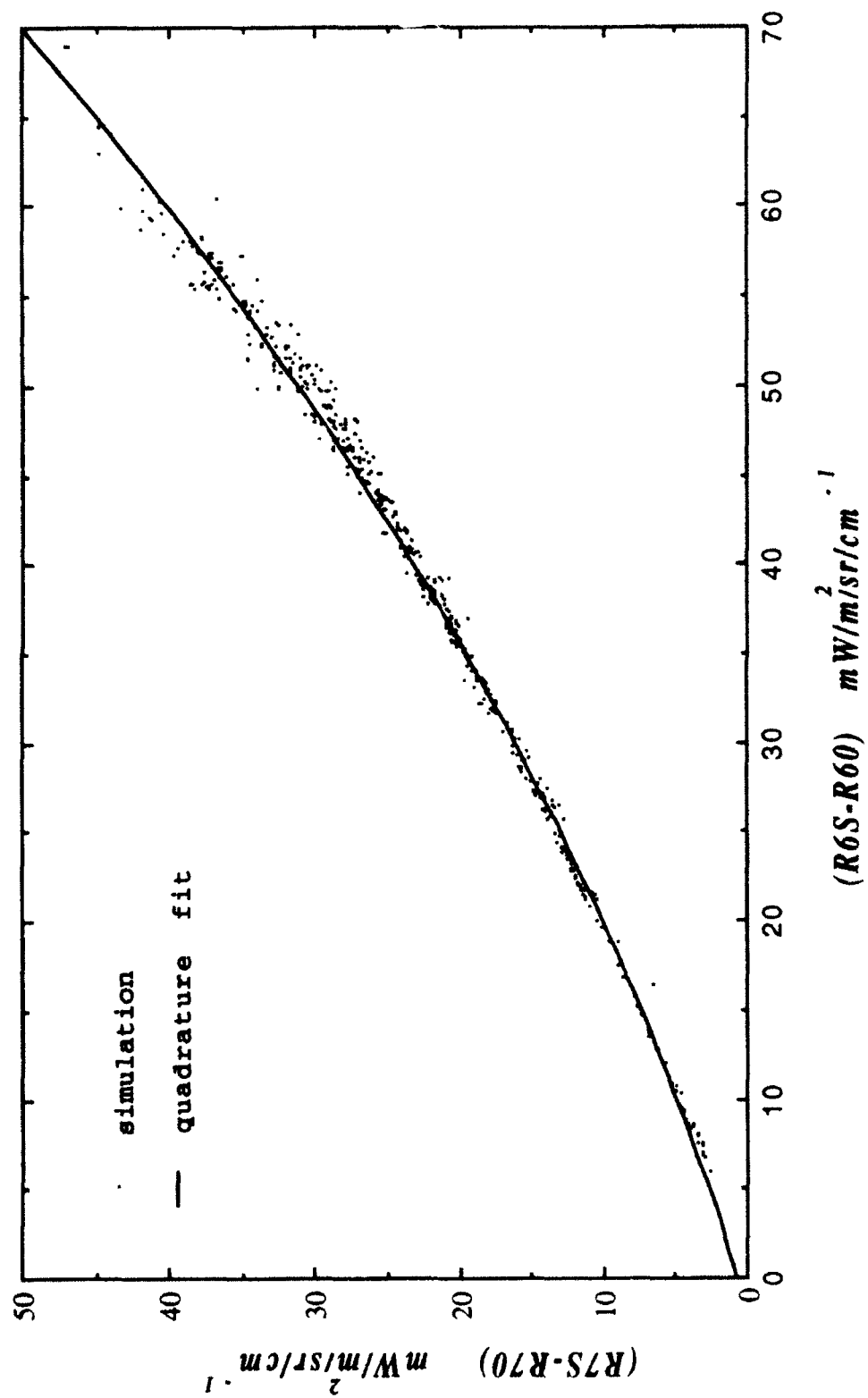
20

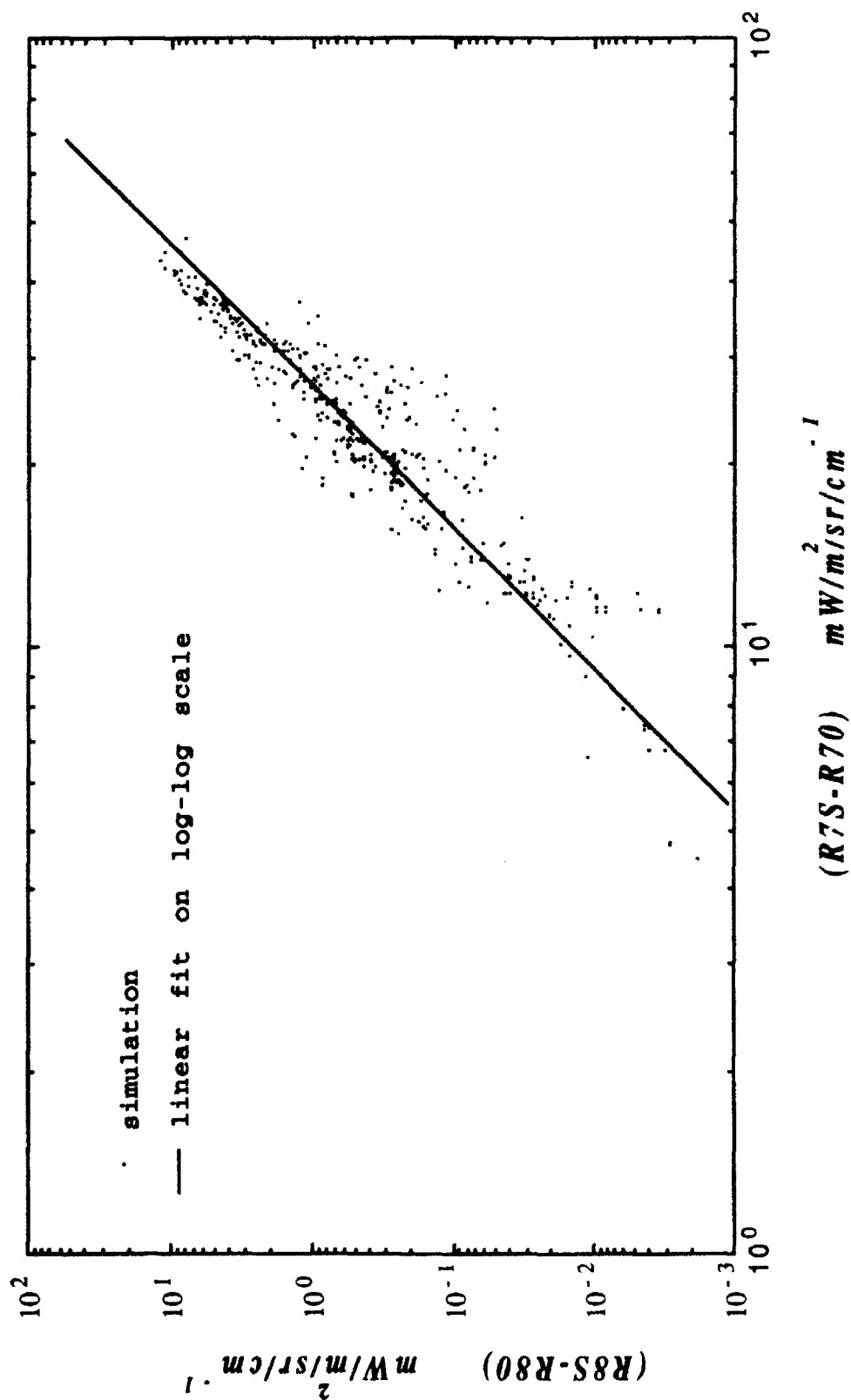Fig. 4   Correlations (a) between ΔR_7 and ΔR_6 and (b) between ΔR_8 and ΔR_7.

Fig. 4 Continued.

R_{s8} using R_{o8}. A linear regression analysis has been performed, and the ΔR_8 values are correlated with ΔR_7 as follows:

$$\ell n \Delta R_8 = e_o + e_1 \ell n \Delta R_7, \qquad (4.5)$$

where $e_o = -14.33$, and $e_1 = 4.35$.

4.2.2 Relationship Between Partly-Cloudy Radiances of Selected Channels

The N^*-method is based on the assumption that the partly-cloudy radiances for a particular pixel is a linear function of the cloud cover η. Given that N^* is constant for all channels, we may derive from Eq. (4.2) the following equation:

$$\frac{R_{oi} - R_{i1}}{R_{oj} - R_{j1}} = \frac{R_{oi} - R_{i2}}{R_{oj} - R_{j2}} = G_{ij}. \qquad (4.6)$$

In the two-dimensional space of R_i and R_j, G_{ij} is the slope of the straight line connecting the points (R_{j1}, R_{i1}), (R_{j2}, R_{i2}), and (R_{oj}, R_{oi}). Further mathematical manipulations of Eq. (4.6) lead to

$$G_{ij} = \frac{R_{i1} - R_{i2}}{R_{j1} - R_{j2}}. \qquad (4.7)$$

The unknown R_{oi} and R_{oj} are eliminated, so that G_{ij} can be estimated from known values of R_{i1}, R_{i2}, R_{j1} and R_{j2}. Once G_{ij} is obtained, a linear relationship between R_{oi} and R_{oj} can be established for either of the adjacent pixels based on Eq. (4.6). This linear relationship can be used in conjunction with the correlation of clear radiances to solve for clear radiances. However, Eqs. (4.6) and (4.7) are valid only when the assumptions made in the N^*-method are valid, i.e., the cloud properties are the same over adjacent pixels. Thus, to apply the multi-spectral method, we must select the most appropriate value of G_{ij} among a sample of adjacent pairs. This is described in the next subsection.

23

4.2.3 Estimate of G_{ij}

Figure 5 illustrates the principle including the optimal estimate for G_{ij}. Shown in the diagram is a two-dimensional display of Chs. 6 and 7 radiances. The inset in the lower-right portion of the diagram is a 3x3 array of numbered pixels. The 3x3 array represents one basic working unit of the cloud removal scheme. Eight pairs of adjacent pixels are formed by pairing the center pixel (#9) with eight surrounding pixels. The nine radiance points corresponding to the pixels are plotted along with the Planck intensity curve. These radiances are assigned based on physical principles. They are smaller than the corresponding clear radiances (R_{o7}, R_{o6}). Because Ch. 7 is more transparent than Ch. 6, $R_{o7} > R_{o6}$, all partly-cloudy Ch. 7 radiances are also larger than Ch. 6 radiances. It is also noted that since the wave numbers of Chs. 6 and 7 are very close, the Planck intensity curve almost coincides with the curve $R_6 - R_7$. The partly-cloudy radiance points do not fall on a single straight line. The distribution of radiances thus signifies a typical situation of different cloud properties for different pixels. This situation frequently occurs in the real data. We note that the point for clear radiances is denoted as "0", which also falls on the curve denoting the correlation between clear radiances (Section 4.2.1). The clear radiance curve intersects the Planck intensity curve at the point (R_{s6}, R_{s7}), which corresponds to the surface emission. Among the partly-cloudy radiance points, point #3 and #9 show the largest difference. The slope of $\overline{93}$ (the straight line connecting #9 and #3) is close to that of $\overline{90}$. Using the slope of $\overline{93}$ as G_{76}, we obtain a solution for the clear radiance at 0' (intersect between $\overline{93}$ and the clear radiance curve). Evidently, 0' is different from 0. However, this solution is more accurate than the solution obtained by using the slope of other straight lines that connect point #9 with other points. Thus, in practice, we select the pair that has the largest difference in Ch. 7 radiances,
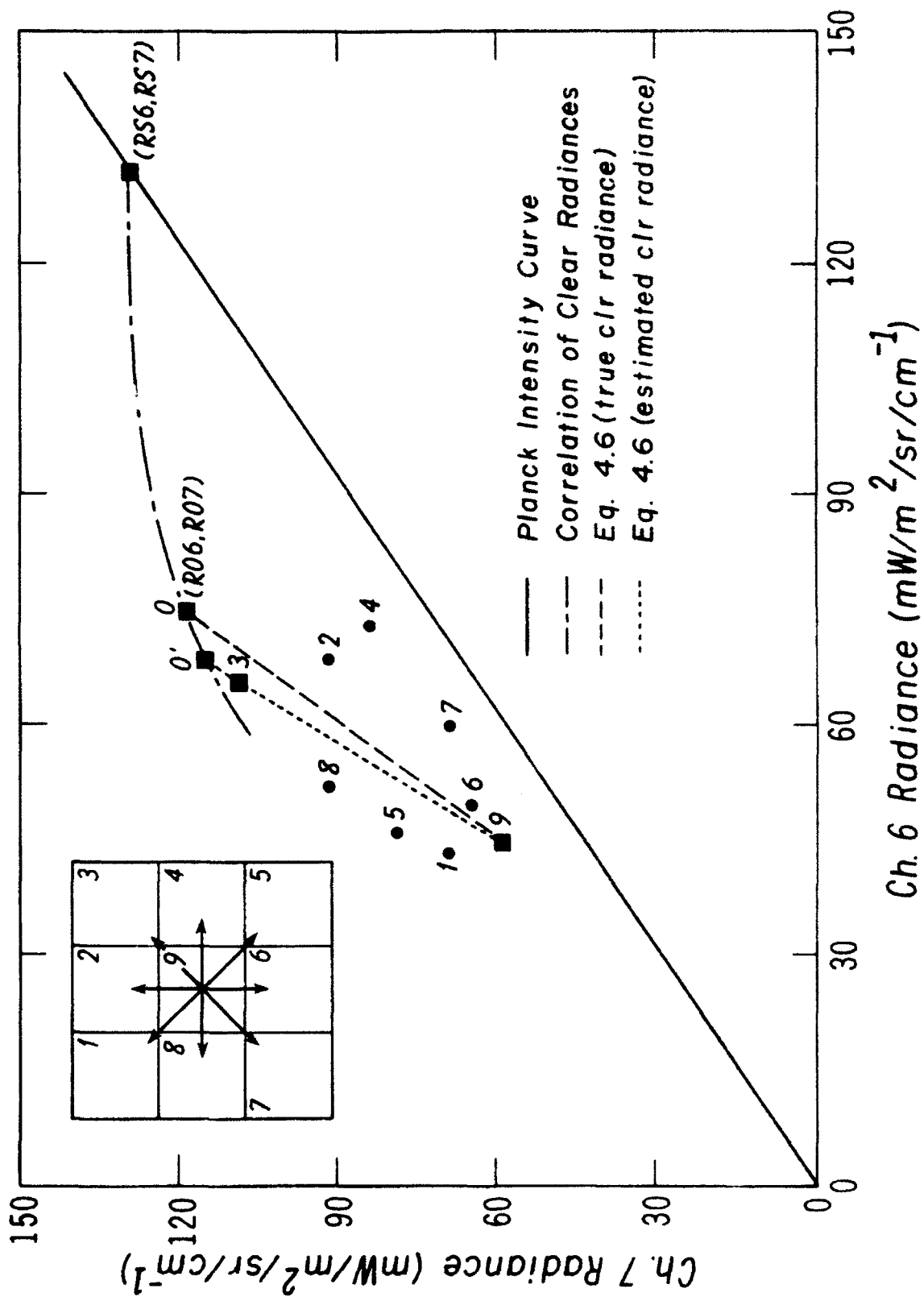
Fig. 5   Conceptual diagram illustrating the strategy for selecting the optimal pair of pixels and the associated G_{ij}.

and compute its associated slopes G_{76} and G_{87}. This strategy does not guarantee the accuracy of the derived clear radiances, however. In particular, if all the radiance points are close to each other, the slope G_{ij} determined according to this strategy may still have a large error. Thus, additional restrictions are required to assume that the determined G_{ij} value is reasonable.

We have performed another set of simulation studies. First, the cloud cover and cloud-top pressure is prescribed randomly for each pair of (R_{o6}, R_{o7}). Next, the clear radiances were computed for the clear radiance correlation (Section 4.2.1). The cloudy radiances are then computed based on the following equation:

$$R_{ci} = B_{\nu}(T_c)T_{\nu}(p_c) + \int_{P_c}^{0} B_{\nu}(p) \frac{\partial T_{\nu}(p)}{\partial p} dp, \quad i = 6, 7, 8, \tag{4.8}$$

where p_c and T_c are cloud-top pressure and temperature, respectively. Partly-cloudy radiances are obtained from Eq. (4.1a). Finally, G_{76} is obtained from Eq. (4.6) using the simulated clear and partly-cloudy radiances. (The simulated values of G_{76} and G_{87} are between 1.0 and 3.0. Also, G_{ij} increases with p_c.) Based on this analysis, any G_{ij} determined from Eq. (4.7) with a value larger than 3.0 or less than 1.0 is rejected.

Finally, we combine Eqs. (4.4), (4.5), and (4.6) to solve for clear radiances of Chs. 6, 7, and 8 and surface temperature simultaneously. A numerical iterative scheme has been developed for this purpose.

Section 5

APPLICATION OF DI TO TEMPERATURE RETRIEVAL

5.1   HIRS Channel Characteristics

In order to investigate the potential applicability of DI, HIRS channels
(Smith et al., 1979) are used to perform the temperature retrieval.   HIRS
consists of 19 channels: Chs. 1-7 are in the CO_2-15 μm band, Ch. 8 is in the 11
μm window band, Ch. 9 is in the O_3-9.6 μm band, Chs. 10-12 are in the water vapor
vibration-rotation band, Chs. 13-17 are in the CO_2-4.3 μm band, and, finally,
Chs. 18-19 are in the 3.7 μm window band.   For the purpose of temperature
retrieval, the seven channels in the CO_2-15 μm band and the five channels in the
CO_2-4.3 μm band will be used. It is noted that the weighting functions of Chs.
1-3 and Ch. 17 peak in the stratosphere ($\bar{p} \leq 100$ mb).

5.2   Parameters of Weighting Functions

We use the generalized weighting function defined in Eq. (2.15) in
conjunction with retrieval analysis. The key parameters in this function are κ
and $\bar{p}$.   Because the weighting function depends slightly on atmospheric
temperature and humidity profiles which are not known before retrieval, accurate
values of κ and $\bar{p}$ cannot be computed in advance.   For this reason, we use
constant values of κ and $\bar{p}$ in the retrieval.   To prescribe κ and $\bar{p}$, the BUAN
temperature and humidity profiles and the NESDIS transmittance model are used to
compute a large number of weighting function profiles for HIRS Chs. 1-7 and Chs.
13-17.   We then use the numerical method previously developed to fit each
weighting function to the generalized form to determine κ and $\bar{p}$ (Ou and Liou,
1989).   Subsequently, we average all κ and $\bar{p}$ values for each channel to obtain
mean values.   Figure 6 shows the average values of κ and $\bar{p}$ for each channel
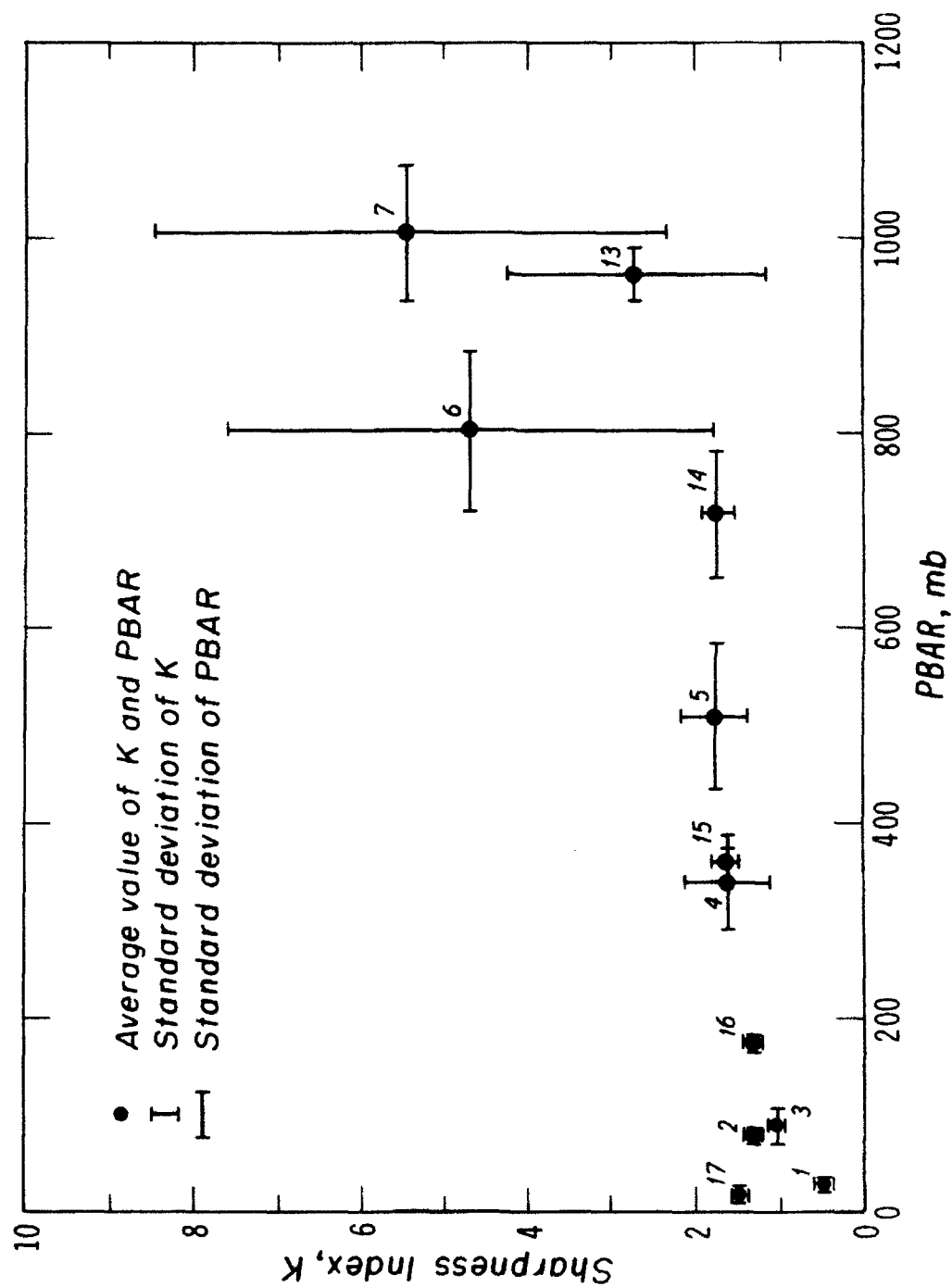
Fig. 6   Distribution of the mean sharpness index $\bar{\kappa}$ and the peak pressure $\bar{p}$. The vertical and horizontal bars denote standard deviation for κ and p, respectively. The numerals denote the channel number.

along with the standard deviations of these values in terms of horizontal and vertical bars. It is evident that the κ values for Chs. 1-5 and 14-17 are smaller than 2 with standard deviations less than 0.5. In contrast, these values for Chs. 6, 7, and 13 are all greater than 2 with standard deviations larger than 1.5. Since Chs. 6, 7, and 13 are affected by the effects of water vapor absorption/emission, variation in κ is primarily associated with variation in the humidity profile near the surface. The range of $\bar{p}$ is generally within 70 mb of the mean values. The tropospheric channels have larger standard deviations in $\bar{p}$ than the stratospheric channels. This indicates that effects of variations in $\bar{p}$ are not negligible for tropospheric temperature retrievals. To incorporate the effects of variation in κ and $\bar{p}$, an iterative approach is required to simultaneously retrieve both humidity and temperature profiles.

5.3 Optimal Degree of Polynomial Fitting of Radiances

Based on our previous investigation, the selection of the degree of polynomial fitting is a critical factor for the successful application of DI to temperature retrieval. Liou and Ou (1988) have tested the accuracy of the retrieved temperature profiles by using different degrees of polynomials in the synthetic retrieval exercises. They found that by utilizing the radiances of the first seven HIRS channels, the fifth-degree polynomial fits almost exactly all the radiances and yields the most accurate retrievals. Figure 7 illustrates the principles behind the selection of the optimal degree of polynomial fitting. The radiances of the first seven HIRS channels are fitted to polynomials of different degrees (third, fifth, and sixth). Mathematically, the accuracy of the fitting is directly proportional to the degree of the polynomial used in the fitting. The sixth-degree fitting is the exact fit for the seven radiances. An important assumption in DI, however, is that the functional form representing the radiance
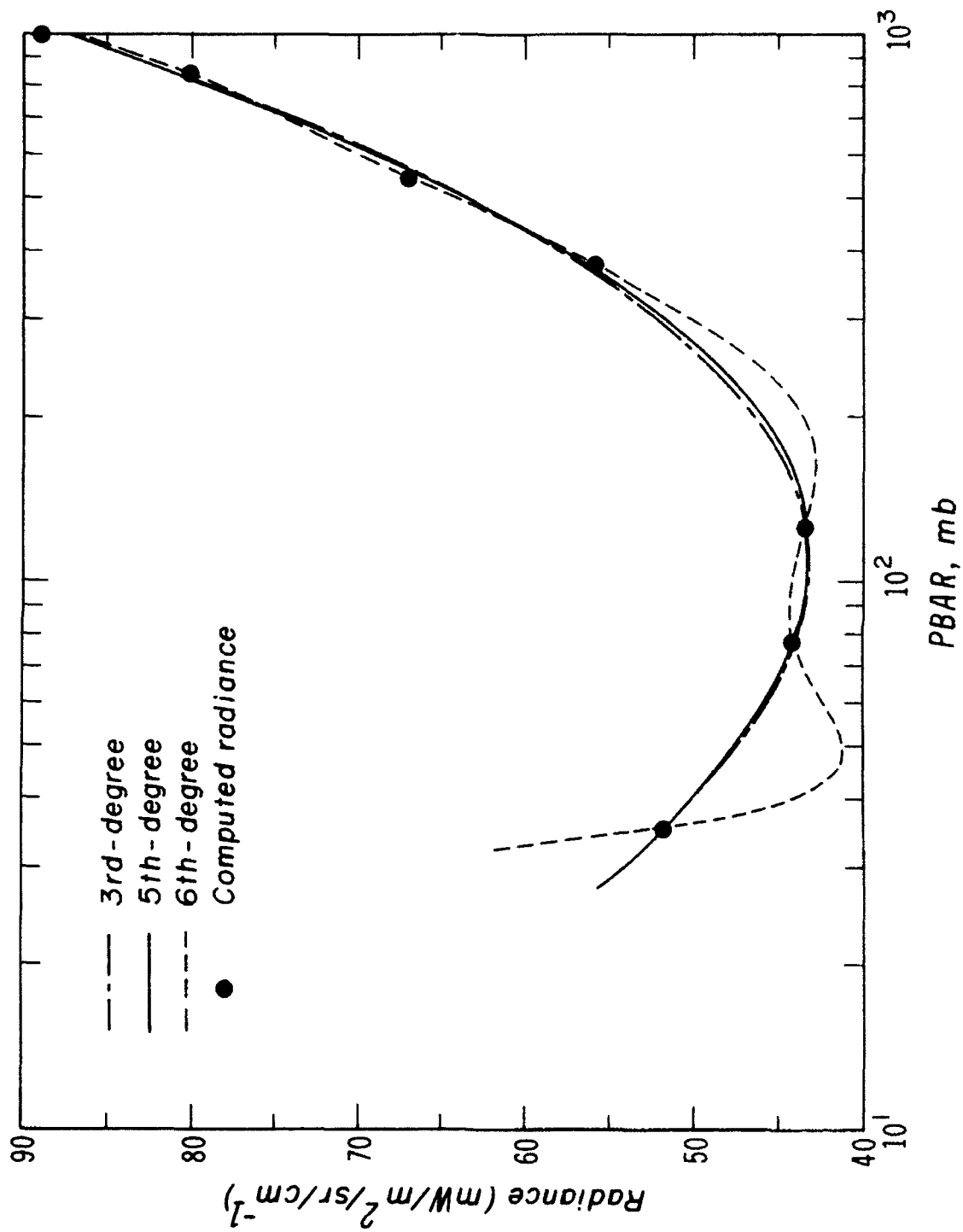
Fig. 7   Fitting of the simulated radiances for HIRS Chs. 1-7 by 3rd-, 5th-, and 6th-degree polynomials.

profile must be smooth. From this figure, it is evident that the sixth-degree polynomial shows fluctuation between points while the fifth-degree polynomial is much smoother. In view of the preceding, the selection of the optimal degree of the polynomial is based on a combination of the smoothness of the polynomial and the accuracy of the fitting. If the number of channels increases, it is expected that the optimal degree of polynomial fitting will be higher. We have chosen the fifth-degree polynomial as an initial attempt to investigate the applicability of DI to temperature retrievals. Our previous research has demonstrated that the fifth-degree polynomial fittings lead to acceptable retrieval accuracy. Further investigations are required for developing a systematic method to determine the optimal polynomial degree.

5.4   Adjustment of Radiances

Previous synthetic retrieval studies show that applications of the DI using simulated HIRS radiances without adjustments produce large errors (~5 K; Ou and Liou, 1989). These errors occur because the problem of remote sounding of temperature is nonlinear. The main sources of nonlinearity are (Houghton et al., 1984):

- dependence of the transmittance on temperature

- dependence of the Planck intensity on wave number within the spectrum of a sensing channel

- dependence of the Planck intensity on wave number between spectral bands

- dependence of the transmittance on the concentration of absorbing gases and aerosols

- model constraints

- effects of clouds

31

The first of these sources is relatively weak, but other factors may significantly affect retrieval accuracy. We have already described a method to remove cloud contamination in satellite data in the previous section. Clear radiances are obtained either by using values of an identified clear pixel or by applying the cloud-removal procedure involving a partly-cloudy pixel. To obtain satisfactory retrieval results, these clear radiances must be "linearized" in the context of DI. Ou and Liou (1989) have proposed an adjustment scheme in terms of a "scaling factor" which encompasses the effects of variations in the sharpness index, surface discontinuity of temperature, and channel properties. The present adjustment process is based on this scheme. Furthermore, we develop a correlation between original and "linear" radiances. The linear radiances are generated from the weighting function profile with uniform shape (fixed κ) and the Planck intensity profile at a reference wave number, subject to model constraints that are explained in the next paragraph. All the preceding major nonlinear factors may be removed by the procedure. The correlation is not sensitive to variations in temperature and humidity profiles (Ou and Liou, 1989).

An important model constraint of DI is that it is developed for an infinite atmosphere. The real atmosphere, however, is semi-infinite with the surface as the lower boundary. In Section 2, we have demonstrated that the radiative transfer equation for a semi-infinite atmosphere denoted in Eq. (2.1) may be transformed to an equation corresponding to an infinite atmosphere [Eq. (2.4)]. The basic assumption is that the slab below the earth surface may be viewed as a semi-infinite isothermal emitter. This conversion implies that the polynomial expression for the Planck intensity profile [Eq. (2.18)] should cover the whole range of pressure ($p = 0$ to $p \to \infty$). Discontinuity always occurs between the skin temperature and surface air temperature. Polynomial expressions generally cannot adequately represent this discontinuity and the behavior of constant temperature

32

below the surface. Figure 8 illustrates this point. The solid line is the HIRS Ch. 7 Planck profile based on the US Standard temperature profile. Below the surface, temperature is assumed to be constant. Also shown is the Ch. 7 weighting function based on the generalized form. The dashed line is the fifth-degree polynomial which fits the full range of temperature profile for 30 mb < p < 200 mb (W > 0.02). Clearly, this fitting is not satisfactory. Not only is the below-surface constant temperature not able to be simulated well, but significant deviations also occur for the stratospheric profile. The fifth-degree polynomial fitting is much improved, but only for the atmospheric portion. The part of the temperature profile below the surface is not important in retrieval practice. For this reason, we may confine the fitting to the above-surface (p < 1000 mb) temperature profile. The linear radiance is evaluated based on the polynomial expression that closely fits the atmospheric (above-surface) Planck intensity profile.

To correlate the satellite radiances and linear radiances, we use the BUAN temperature profiles and the transmittance model to perform simulations. First, linear radiances are computed. We select 700 cm^{-1} as a reference wave number and use the κ value corresponding to the generalized weighting function of Ch. 7 determined in Subsection 5.2. The 700 cm^{-1} Planck intensity profile based on the atmospheric (p < p_a) temperature field is fitted to a fifth-degree polynomial. Then from Eq. (2.17), the coefficients of the polynomial are determined. Finally, linear radiances are computed from Eq. (2.16).

The simulated radiances are computed from Eq. (2.1) using the weighting functions that are computed from the transmittance model. Figures 9a-l show the distribution of the linear radiances vs. simulated radiances for the 12 channels used in the temperature retrieval. We see that the correlation for each channel is significant, except Ch. 16. Susskind et al. (1983) also noted that the
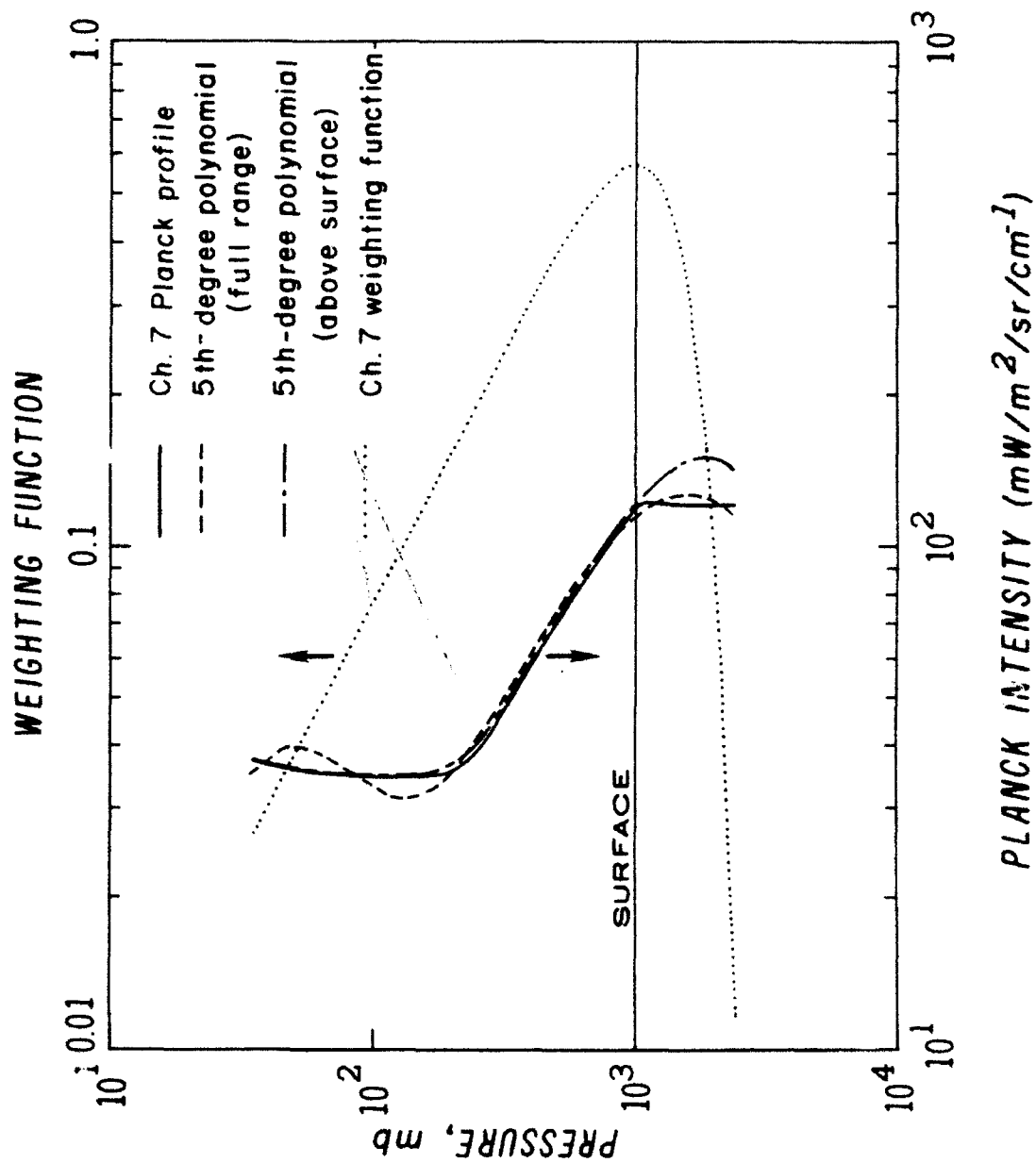
Fig. 8   Fittings of the HIRS Ch. 7 Planck intensity profile base on the U.S. Standard temperature profile. The Ch. 7 weighting function is also shown.
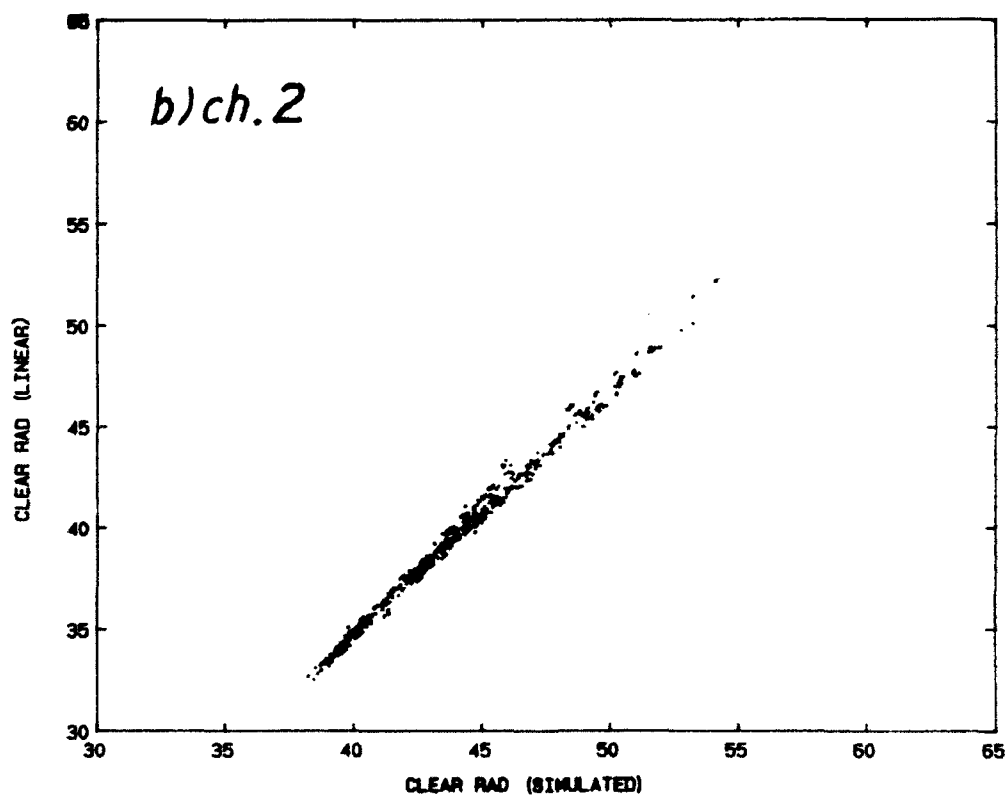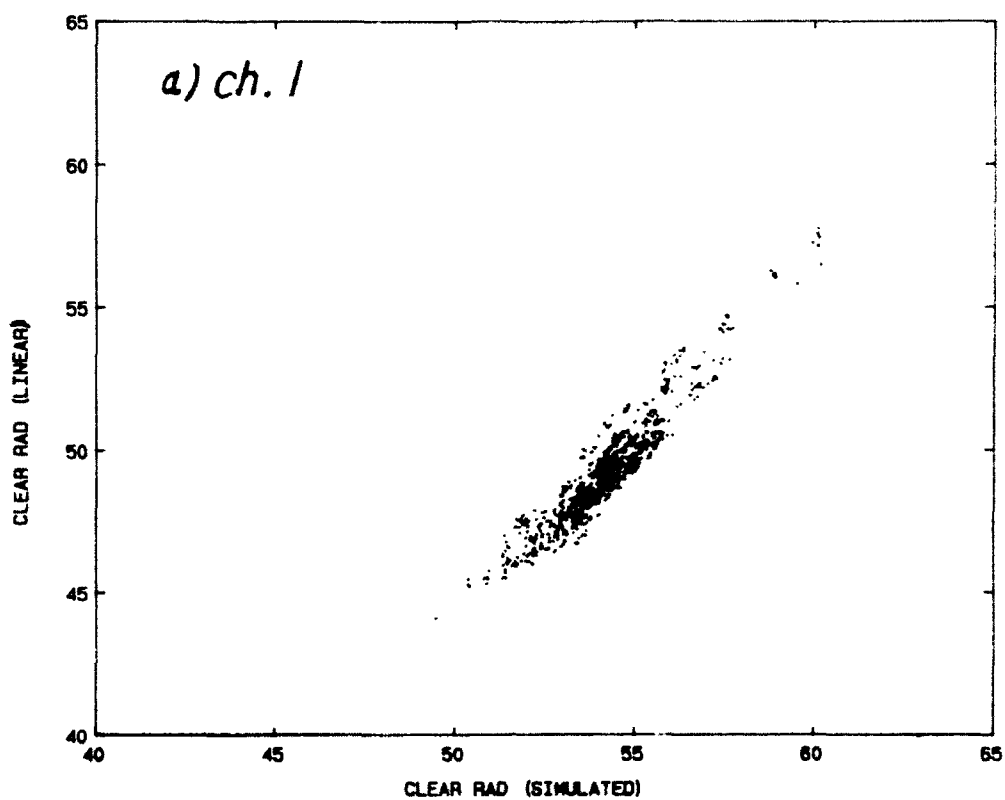
Fig. 9   Correlations between linear and simulated clear radiances for HIRS
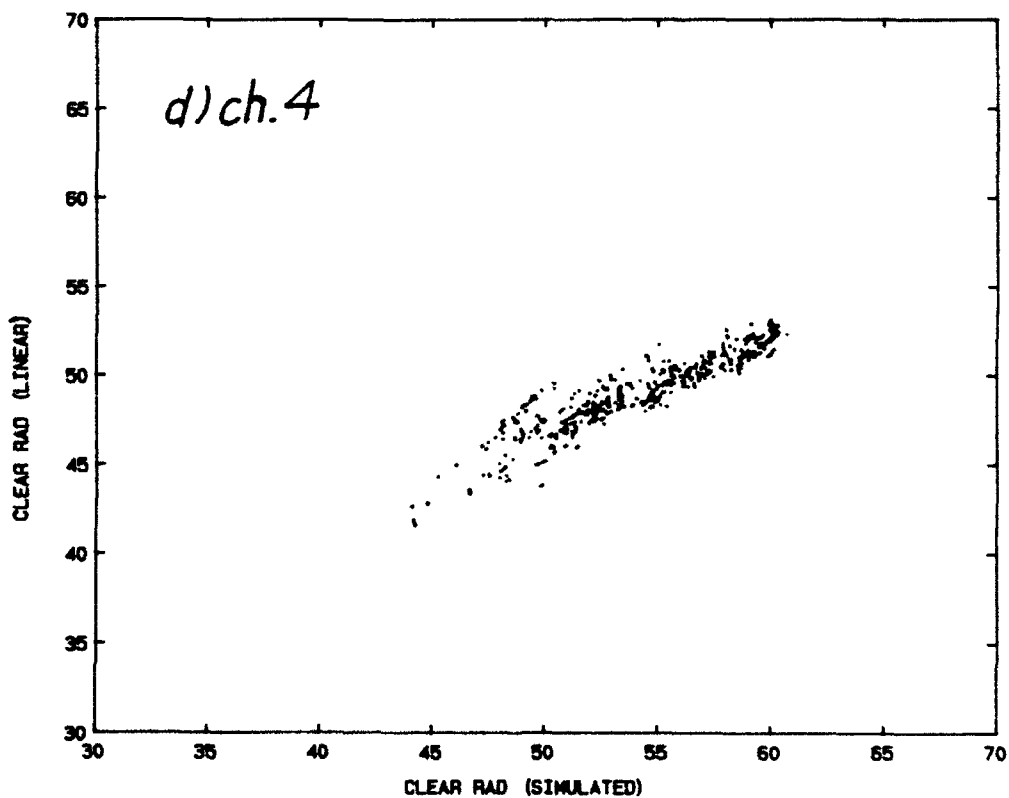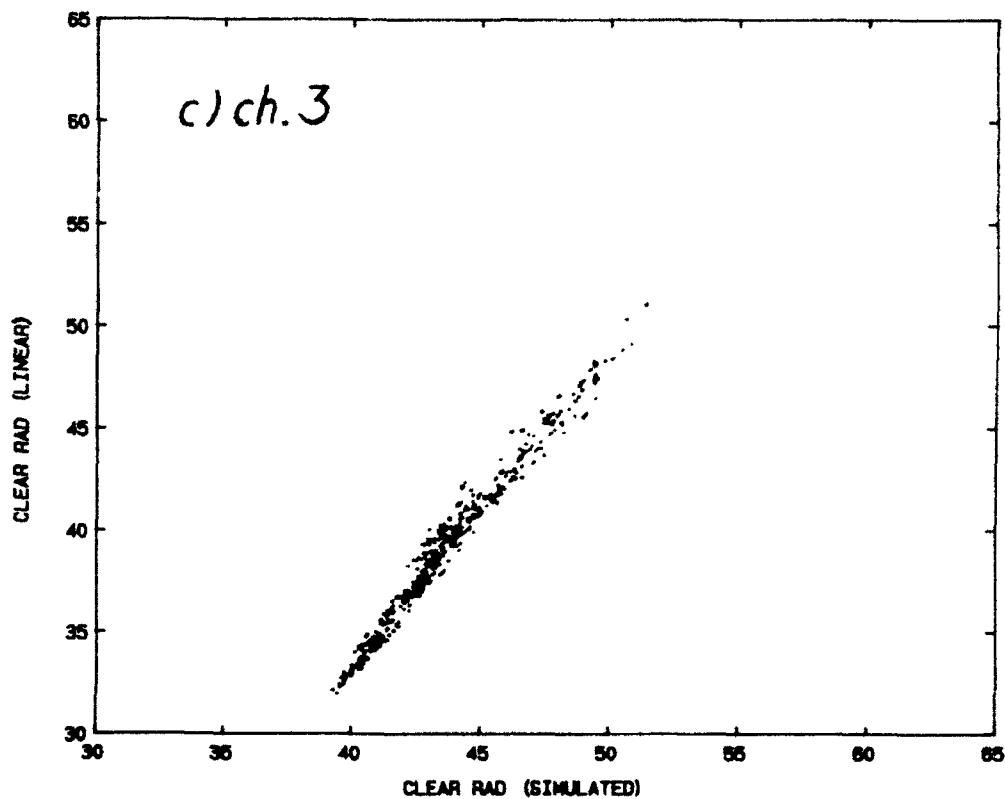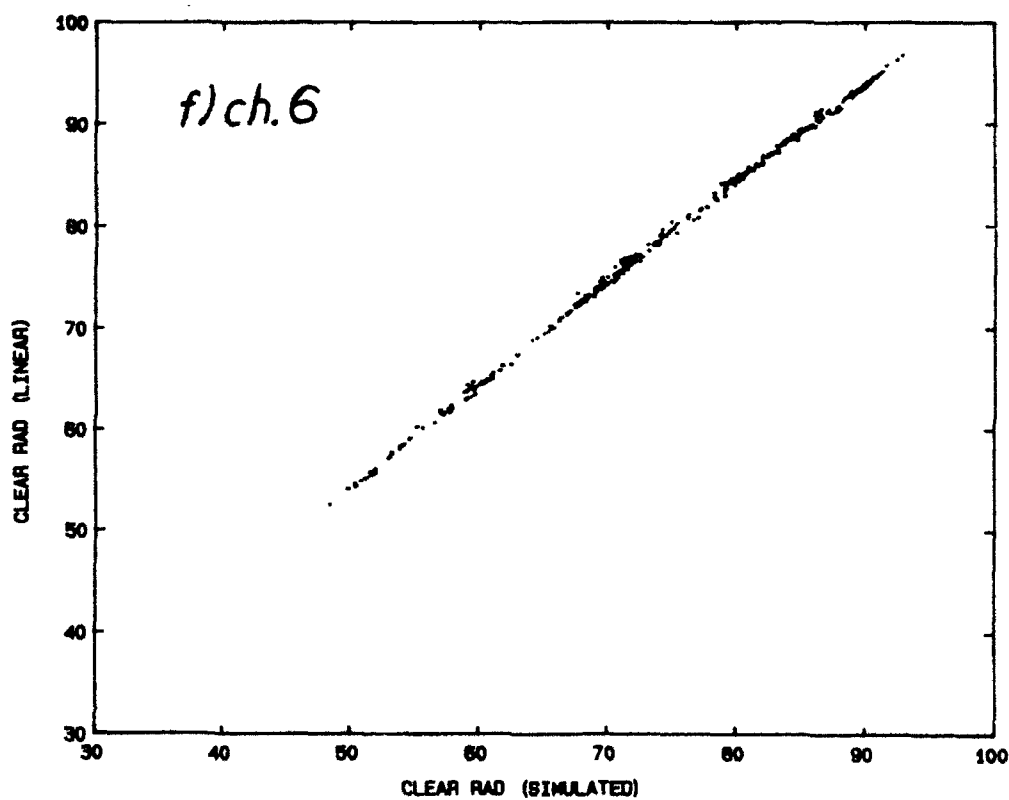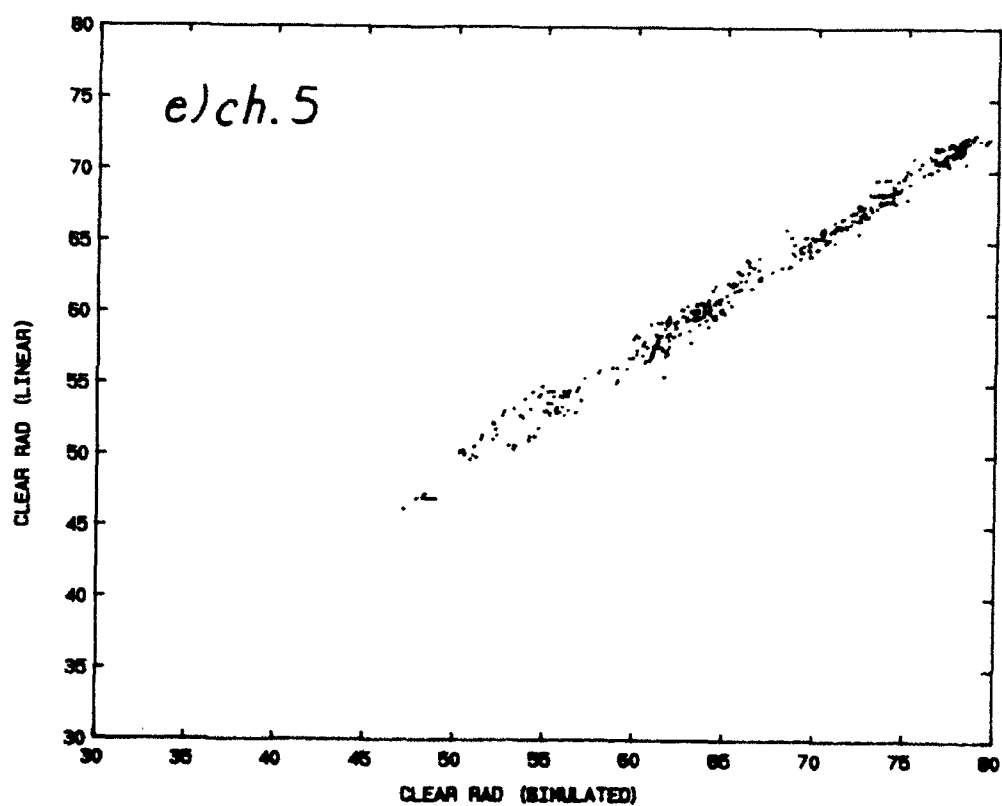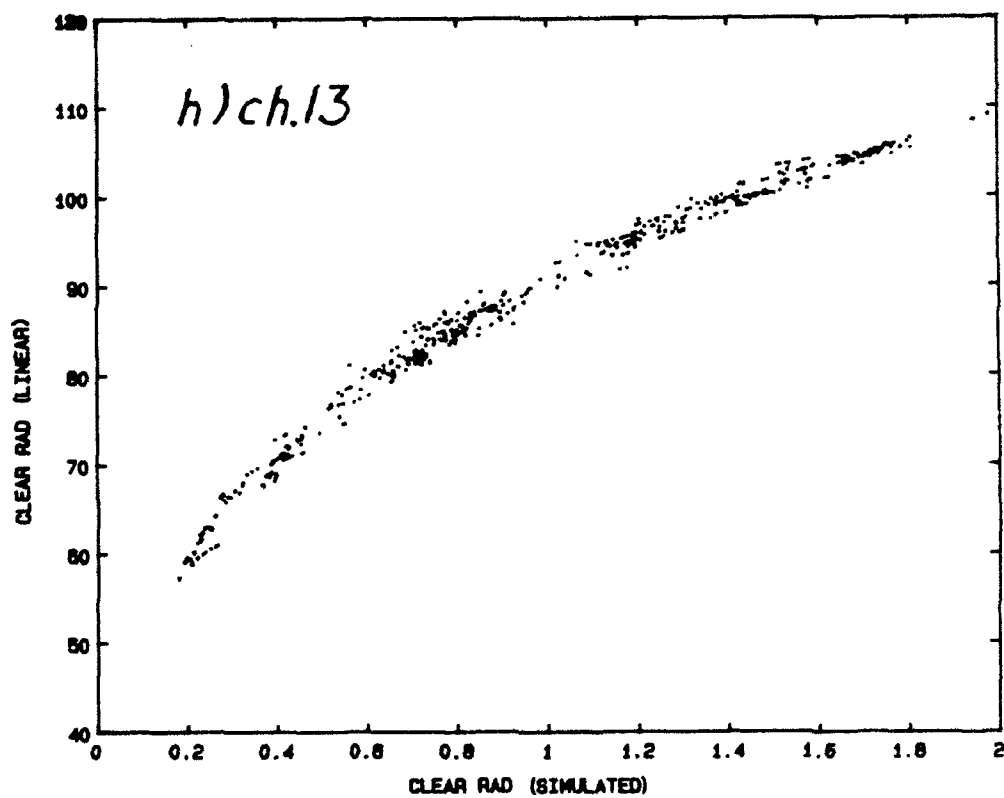   Chs. 1-7 (a-g), and Chs. 13-17 (h-1).

c) ch.3

d) ch.4

Fig. 9   Continued.

Fig. 9   Continued.

g) ch.7

h) ch.13

Fig. 9   Continued.

38

i) ch.14

j) ch.15
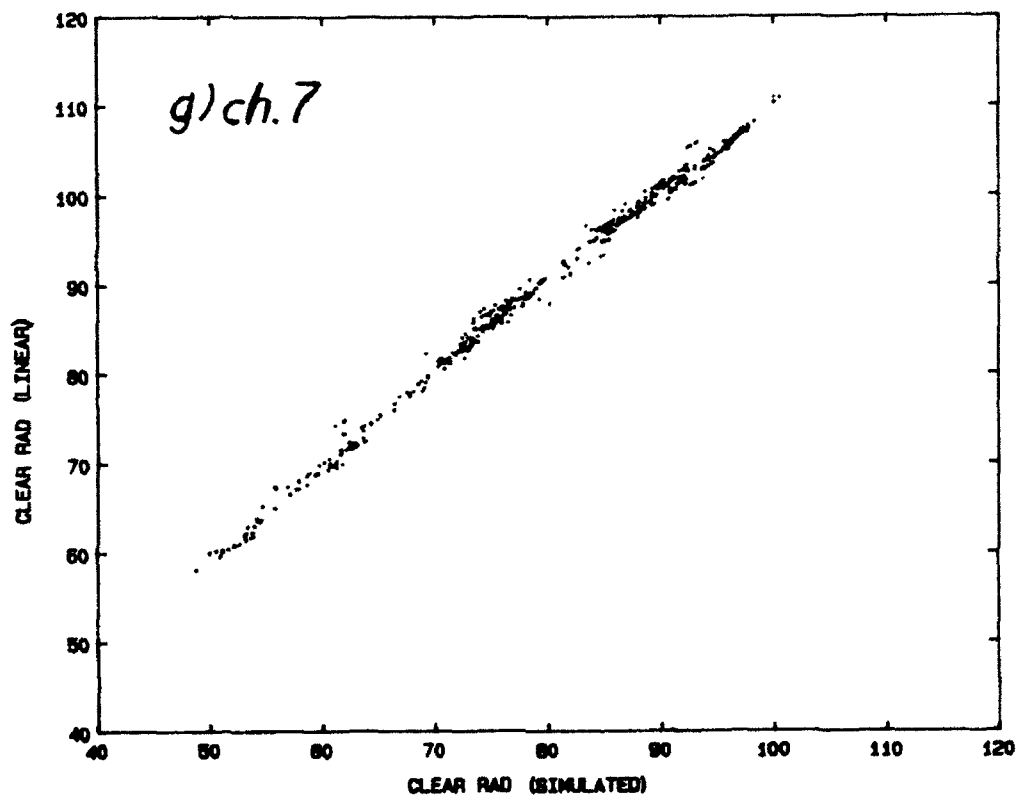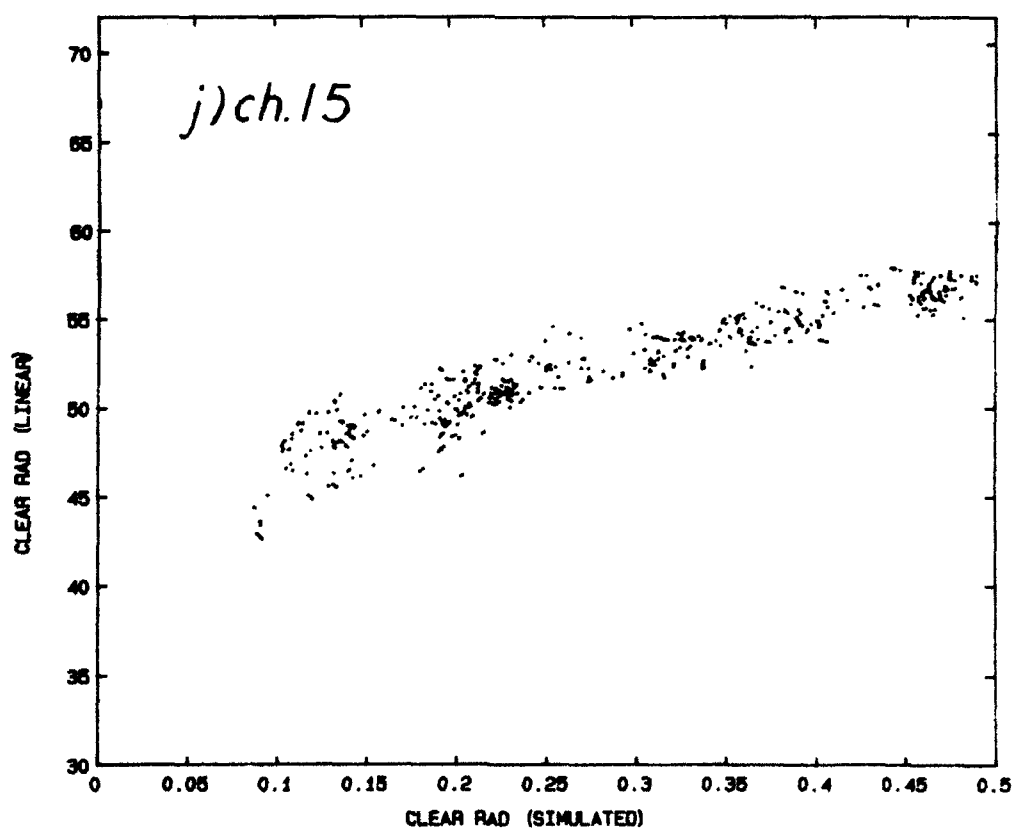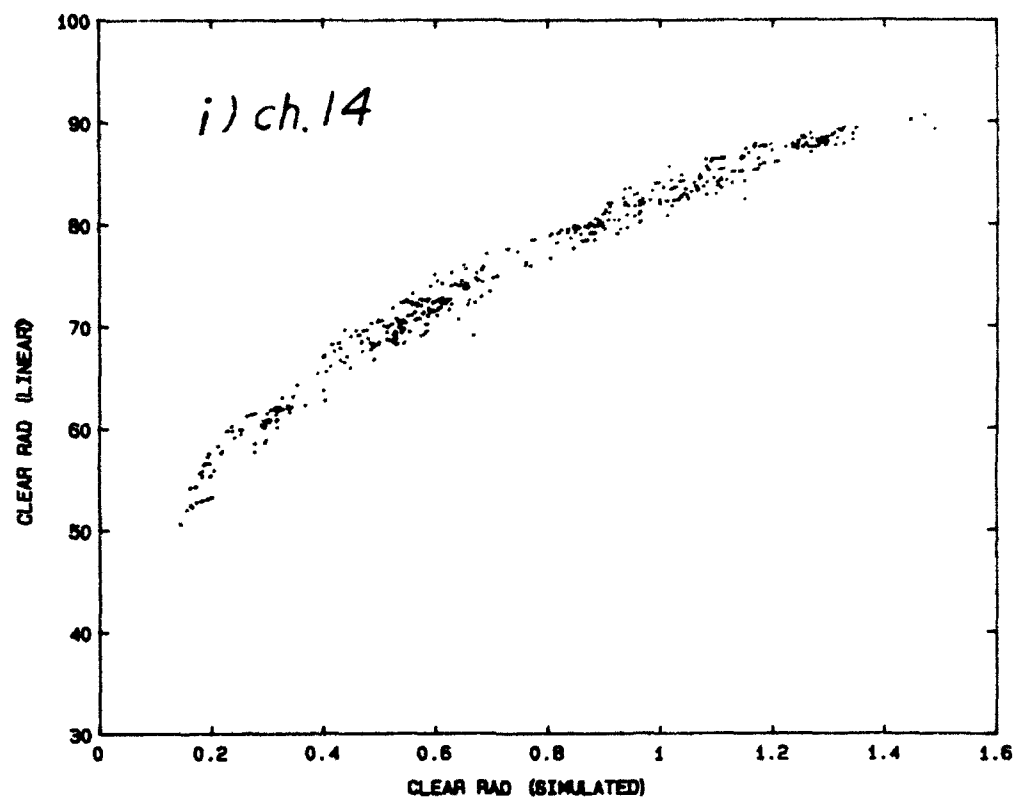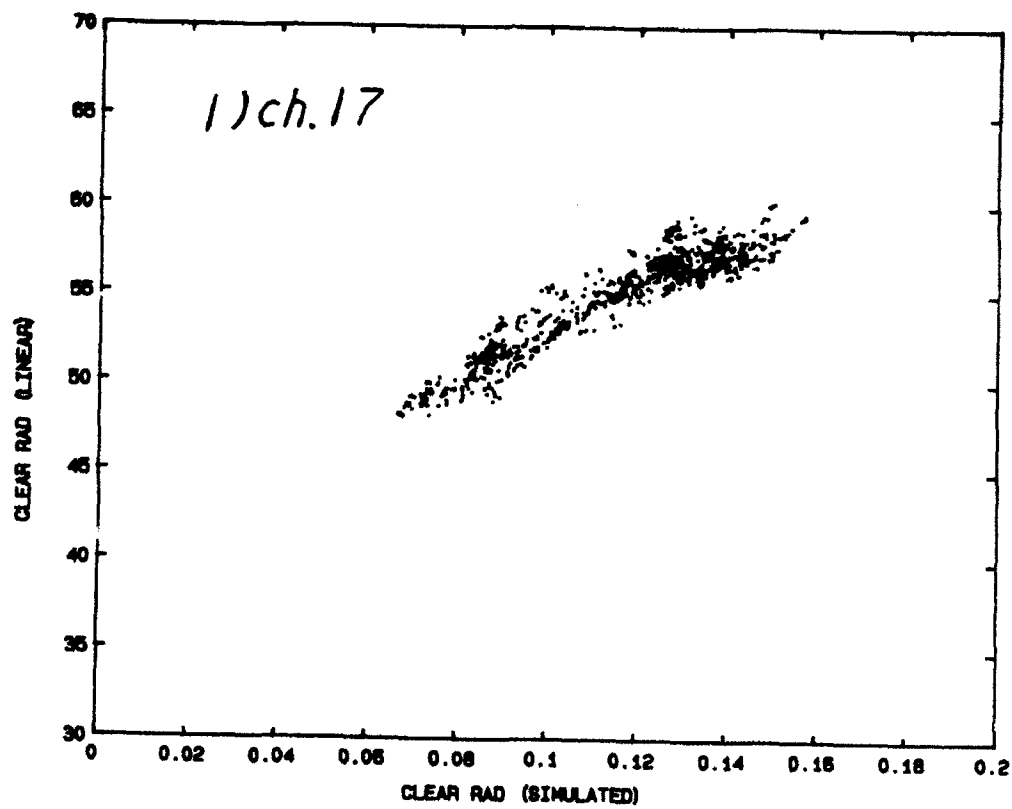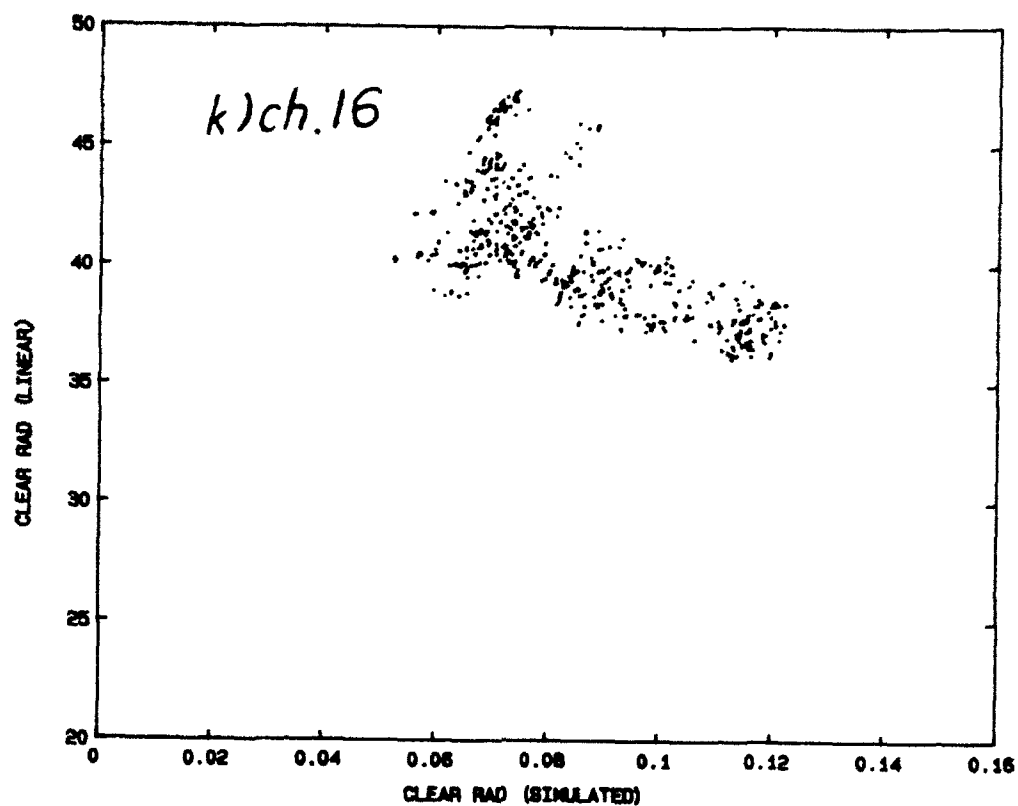
Fig. 9   Continued.

Fig. 9   Continued.

"atmospheric response of Ch. 16 is very diffuse." This may be due to the fact that the weighting function of Ch. 16 peaks near the tropopause at about 200 mb (Fig. 8). In the present retrieval, the data involving Ch. 16 are not used. The radiance correlations for Chs. 6, 7, and 13 are particularly significant, presumably due to the narrow form of weighting function of these channels.

We then perform the regression analysis for each channel in the form

$$R_{i1} = a_i + b_i R_{is} + c_i R_{is}^2, \qquad (5.1)$$

where R_{i1} and R_{is} denote linear and simulated radiances. Table 1 lists the values of a_i, b_i and c_i along with the root-mean-square (rms) differences between the model-computed and fitted values of R_{i1}. The rms differences between linear and simulated radiances are less than 1.3 $mW/m^2/sr/cm^{-1}$, indicating that the linear and simulated radiances are highly correlated. The coefficients a_i, b_i and c_i depend on the functional form of weighting function, the reference wavenumber

Table 1   Coefficients in the correlation between the simulated and linear radiances and root-mean-square differences between computed and linear radiances.

Ch.	a	b	c	rms diff. $(mW/m^2/sr/cm^{-1})$
1	101.22	−3.16	0.0407	0.62
2	−16.66	1.35	−0.0016	0.37
3	−70.85	3.46	0.0214	0.60
4	−9.19	1.68	−0.0110	0.91
5	10.96	0.75	0.0004	0.74
6	−2.53	1.21	−0.0016	0.28
7	−3.51	1.37	−0.0024	0.77
13	51.30	51.63	−12.02	1.29
14	46.65	51.26	−14.92	1.26
15	42.41	45.68	−33.45	1.22
17	31.26	303.30	−827.9	0.86

and the degree of polynomial for the linear radiances. These coefficients are insensitive to temperature profiles, however. The set of coefficients shown here only represents an example of the correlation between simulated and linear radiances. Note that different reference wave number, sharpness index, and polynomial will produce different correlation equations. Further studies are required to search for the optimal correlation.

Section 6

RETRIEVAL RESULTS AND DISCUSSIONS

Using the BUAN collocated satellite and radiosonde data, we have performed retrievals to investigate the applicability of the DI to satellite data. The data consists of 1000 profiles selected for this study which were collected between April 3 and April 7, 1988, and these profiles encompass the entire globe. Based on the N^* values given in the BUAN data, the profiles have been separated into three groups: clear ($N^* = 0$), partly cloudy ($0 < N^* < 1$), and overcast ($N^* > 1$). Table 2 lists the geographical distribution of the selected data. More than half of the cases are clear. About 20% of the cases are identified as partly cloudy. About 33% of the cases occur over the northern midlatitude area (60°N-30°N), while about 80% of the cases occur over the oceans.

Temperatures are computed for each peak pressure level of the weighting functions between 17 and 100 mb. There are eleven layers between these levels. For each of the ten layers between 28 and 1000 mb, two-point averages are applied to obtain layer-mean values. The top layer between 17 and 28 mb has not been

Table 2   Geographical distribution of selected data.

Geographical Zone	Number of Profiles			
	Clear	Partly Cloudy	Overcast	Total
90°N-60°N	168	36	36	240
60°N-30°N	130	91	101	322
30°N-30°S	173	47	56	276
30°S-60°S	66	10	36	112
60°S-90°S	23	13	14	50
ocean	472	158	171	801
land	88	39	72	199
Total	560	197	243	1000

selected for presentation because of the large temperature differences in this layer. The large temperature differences are due to errors in polynomial fitting for p < 17 mb. The purpose of averaging is to simulate the vertical resolution of the input temperature field for weather prediction models. These models are usually initialized using layer-mean rather than level temperature values. In addition, differences between retrieved and sounding values are smaller based on layer-means than based on level values because of the smoothing effect of the averaging process.

Differences between retrieved and sounding layer-mean temperature values are computed. The sounding values have been obtained by interpolation of the BUAN temperature values of the 15 mandatory and 25 significant levels. However, data are not available at some levels. For example, Table 3 lists the number of clear cases for each layer and the geographical zone where sounding values are available. By comparing the first column of Table 2 with Table 3, it is noted that about 10% of the cases in the troposphere are data-void. The reason for these missing data is unknown. Computation of differences can only be carried out at those levels where sounding values are available.

Simulation retrievals are carried out using the linear radiances as input. The purpose is to examine the effects of errors in polynomial fitting on the retrieval performance. Linear radiances have been generated according to the method described in Subsection 5.4. Theoretically, if the Planck intensity profile based on the soundings can be represented by a polynomial in an exact manner, then the retrieved temperature values will be exactly identical to the soundings. Because the Planck intensity profile cannot be exactly expressed in terms of a polynomial, retrieved values differ from the soundings. Table 4 lists the mean differences for each layer and the geographical zone. All clear and partly-cloudy cases are included. For each geographical zone, vertical

44

Table 3 Number of clear cases for each layer and geographical zone where sounding values are available.

Layer Index	Pressure Range (mb)	Number of Cases							
		90°N-60°N	60°N-30°N	30°N-30°S	30°S-60°S	60°S-90°S	Ocean	Land	Total
1	28-78	146	70	125	55	9	344	61	405
2	78-93	146	75	125	62	16	356	68	424
3	93-175	159	100	143	66	21	408	81	489
4	175-325	165	100	151	66	23	422	83	505
5	325-375	165	102	152	66	23	425	83	508
6	375-535	165	102	152	66	23	425	83	508
7	535-740	165	102	152	66	23	425	83	508
8	740-815	165	102	152	66	23	425	83	508
9	815-975	165	108	143	58	21	412	83	495
10	975-1000	152	78	120	44	0	329	65	394

Table 4 Mean differences between retrieved and sounding temperature values for each layer and geographical zone where sounding values are available.

Layer Index	Pressure Range (mb)	Mean Temperature Differences (K)							
		90°N-60°N	60°N-30°N	30°N-30°S	30°S-60°S	60°S-90°S	Ocean	Land	All
1	28-78	0.6	0.72	-5.45	-1.68	1.28	-0.91	-0.58	-0.85
2	78-93	-1.78	-1.75	-1.98	-1.74	-1.42	-1.72	-2.17	-1.81
3	93-175	-3.26	-3.13	4.23	0.76	-3.55	-0.62	-1.23	-0.74
4	175-325	-1.1	-0.66	4.95	1.39	-2.13	0.80	1.41	0.93
5	325-375	4.13	3.54	2.06	1.74	3.39	2.99	3.30	3.05
6	375-535	6.08	3.90	-0.92	1.55	6.39	3.09	2.49	2.97
7	535-740	1.43	0.21	-1.74	-0.12	1.41	0.09	-0.34	0.01
8	740-815	-3.35	-2.30	-1.22	-1.28	-2.55	-2.21	-1.92	-2.14
9	815-975	-4.14	-2.07	0.13	-0.98	-1.90	-2.09	-0.88	-1.84
10	975-1000	0.07	0.13	0.91	0.27	0.36	0.27	0.65	0.35

variation of mean difference with pressure shows a systematic pattern. In general, positive values occur near the surface. Groups of negative and positive values occur alternately in the lower troposphere, upper troposphere, and stratosphere. Clearly this is due to systematic errors in the polynomial fitting. The largest positive differences (~6 K) occur between 375 and 575 mb over polar regions. These large values are associated with the location of the tropopause. The polynomial fitting is unable to resolve the sharp inversion near the tropopause. Since the differences are due purely to the mathematical representation of the Planck intensity profile and are systematic, we may subtract these mean differences from the retrieved values to reduce errors. Further studies are required to relate the mean differences to the properties of Planck intensity or radiance profiles.

Comparison of the results from different radiance input reveals the effects of adjustment errors and instrument noises. Simulated radiances have been generated using the BUAN temperature and humidity profiles based on Eq. (2.1), and are adjusted using Eq. (5.1). Similarly, BUAN satellite data are first converted from brightness temperature to radiances and then adjusted using Eq. (5.1). Figure 10 shows the vertical profiles of layer-mean rms temperature differences for retrievals using linear, simulated and BUAN radiances as inputs. All clear and partly cloudy cases are included. The same mean difference values given in Table 4 have been subtracted from the retrieved results according to latitudinal zones for all three input sets. The rms differences for all three sets are about 2 K between 100 and 700 mb. The larger differences (~2.2 - 3 K) for $p < 100$ mb are mainly due to inversions near the tropopause for tropical areas. The rms differences for retrieval using linear radiances are less than 2 K for $p > 100$ mb. These differences are caused by the residual effects of polynomial fluctuation around the sounding profile, after mean differences have
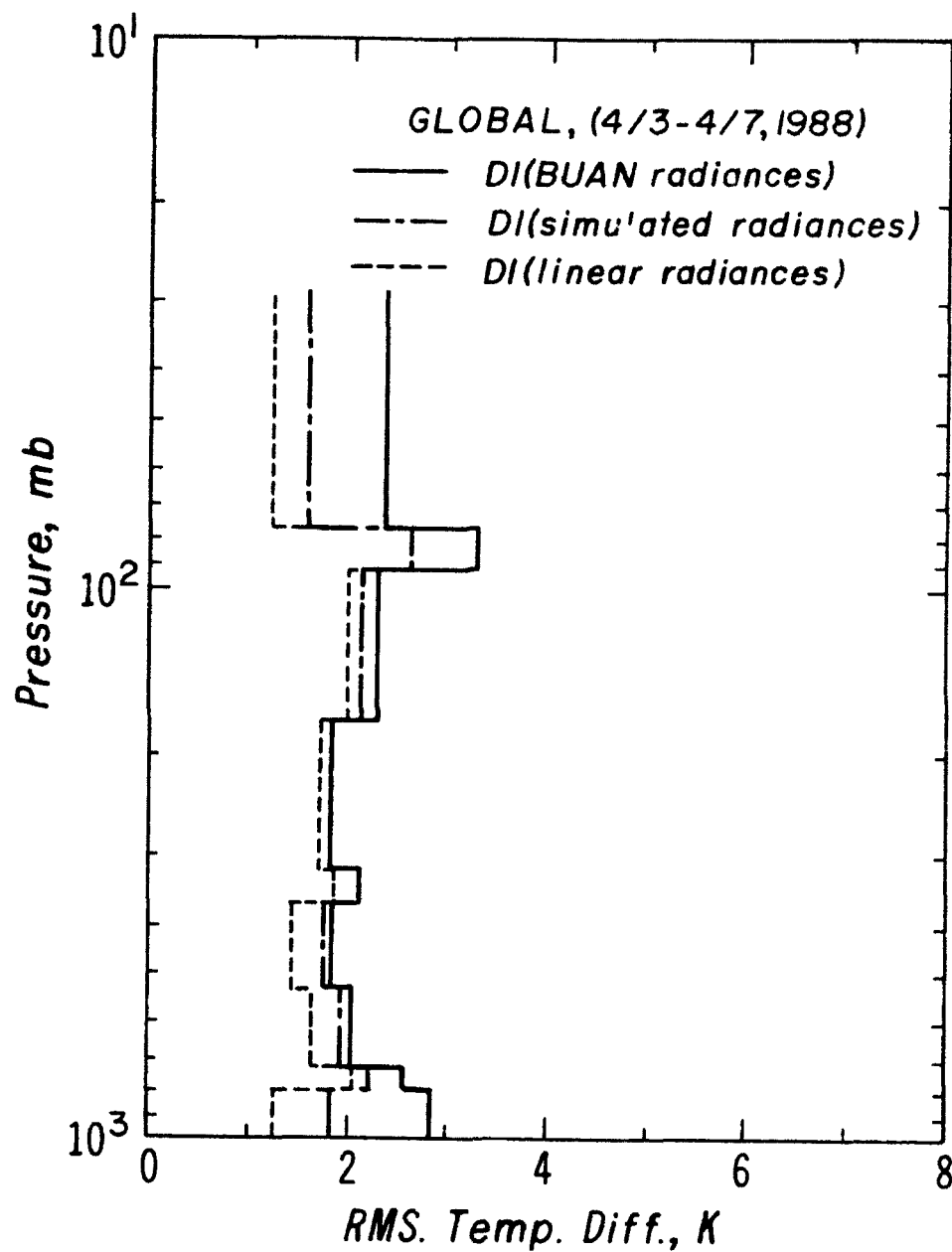
Fig. 10   The vertical profiles of rms differences from temperature retrievals
using linear, simulated and BUAN radiances as input.

been subtracted. The rms differences for simulated radiances are slightly larger (≤ 0.5 K) than those for linear radiances. The increase in rms differences is due to uncertainties in the correlation denoted in Eq. (5.1). Finally, the rms differences for BUAN satellite data are also slightly larger (≤ 1 K) than those for simulated radiances. The increase in rms difference near surface results from the differences between the BUAN and simulated radiances associated with instrument noise and error in the weighting function of the near-surface channels (Chs. 6, 13, and 7). It appears that, between 100 and 700 mb, the effects of correlation, instrument noise and error in the weighting function on resulting rms differences are smaller than the effects produced by polynomial fitting.

To compare the performance of DI with the BUAN retrieval scheme, the vertical profiles of rms differences for the two schemes are shown in Fig. 11. The BUAN satellite data have been used in both schemes. Also shown is the rms differences for the BUAN first-guess values. All clear and partly cloudy cases are included. Except for $p > 800$ mb, the rms differences for the BUAN scheme are between 1 K and 2 K. For $p > 100$ mb, the rms differences for DI are larger than the differences for the BUAN scheme by less than 1 K. For $p > 500$ mb, the larger rms differences for DI are caused by the neglect of the effects of humidity variation near the surface on the weighting functions of Chs. 6, 7, and 13. For 300 mb $< p <$ 500 mb, accuracies of DI and of BUAN scheme are comparable. For $p < 300$ mb, the larger rms differences for DI are produced by uncertainties in the polynomial expressions of temperature values near the tropopause. To improve DI, we must incorporate the effects of humidity in the retrieval and improve the fitting of temperature inversions at the tropopause. The results shown in the diagram indicate that DI is potentially capable of achieving retrieval performances comparable to the BUAN scheme. The DI neither requires a first-guess profile nor uses error covariance matrices to regulate solutions. The rms
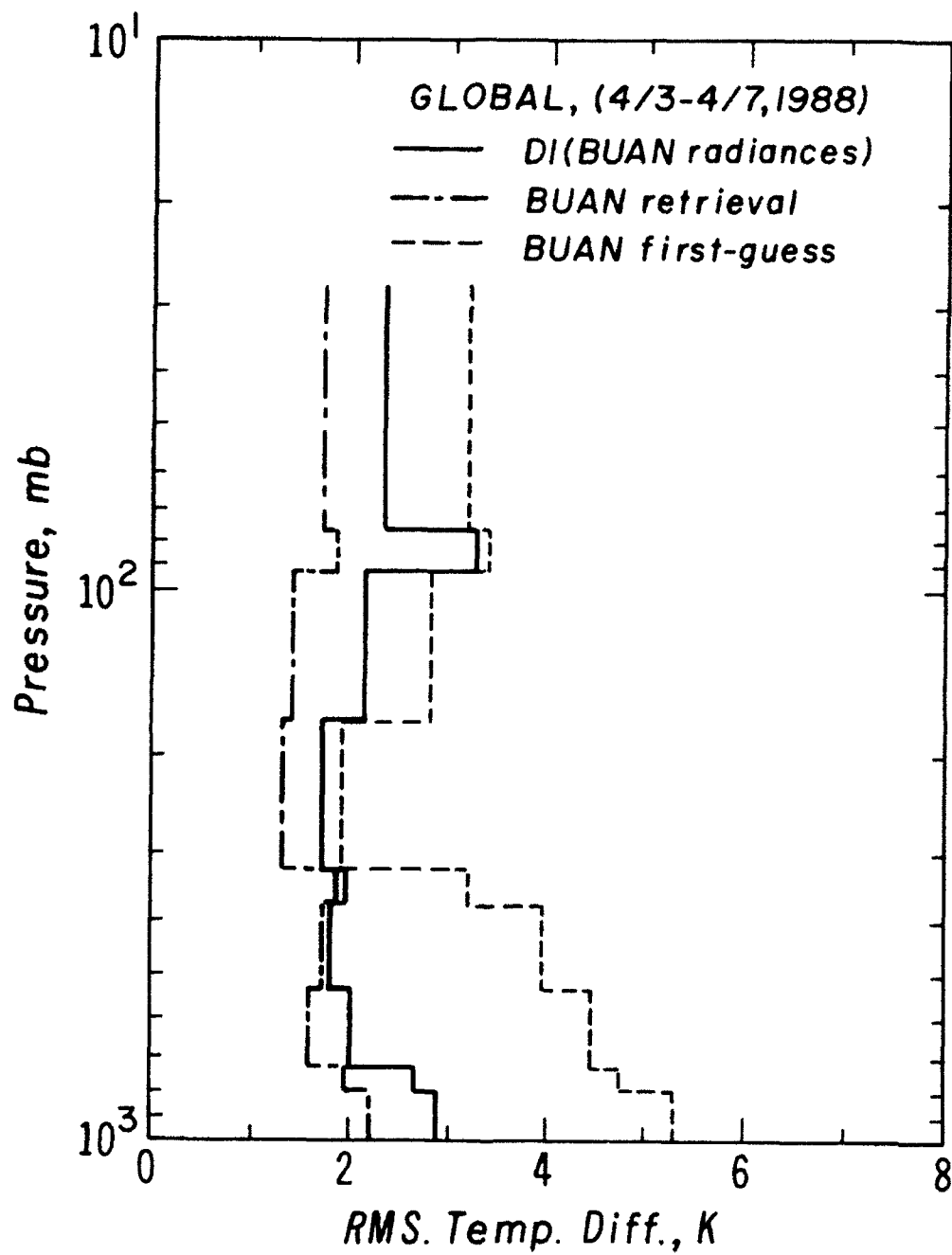
48

Fig. 11   The vertical profiles of rms temperature differences from the DI and
           BUAN schemes, using the same BUAN radiances.

differences for the BUAN first-guesses, as shown in Fig. 11, range between 2 K in the upper troposphere and 5 K near the surface. The rms differences for DI are everywhere less than those for the BUAN first-guesses. Thus, DI can be used as a tool to obtain the first-guess profiles for the minimum-variance method.

To test the proposed multi-spectral cloud-removal scheme described in Section 4, we have also carried out retrievals using DI under partly-cloudy conditions. Figure 12 shows the vertical profiles of rms differences for partly-cloudy retrievals using the DI and BUAN schemes. Two sets of radiances are employed as inputs in DI. One set is the BUAN radiances which were obtained by the BUAN cloud-removal method. The other set is the cloud-removed clear radiances from the multi-spectral method. The rms differences for BUAN first guess profiles are also shown. We have selected about 1/3 of the partly-cloudy cases in which the differences in Ch. 7 radiances for the selected pair of spots for cloud-removal are larger than 20 mW/m^2/sr/cm^{-1}. For the remaining partly-cloudy cases, the assumption involving the same cloud properties may not be satisfied so that the slopes G_{76} and G_{87} will contain large errors. McMillin (1978) also noted that the clear radiances determined for cases with larger differences in the window channel radiance are expected to be closer to true values. Similar to Fig. 11, the rms differences for BUAN retrievals are between 1 and 2 K for p < 800 mb. The rms differences for DI using BUAN radiances are close to those for the BUAN scheme. In fact, between 300 and 500 mb, the DI yields better accuracy than the BUAN scheme. The larger rms differences near 90 mb are due to uncertainty in the retrieved tropopause temperature over tropical areas. By comparing rms differences for DI using two sets of radiances, we see that the present multi-spectral method produces only slightly larger rms differences than the BUAN N*-method (~0.5 K).
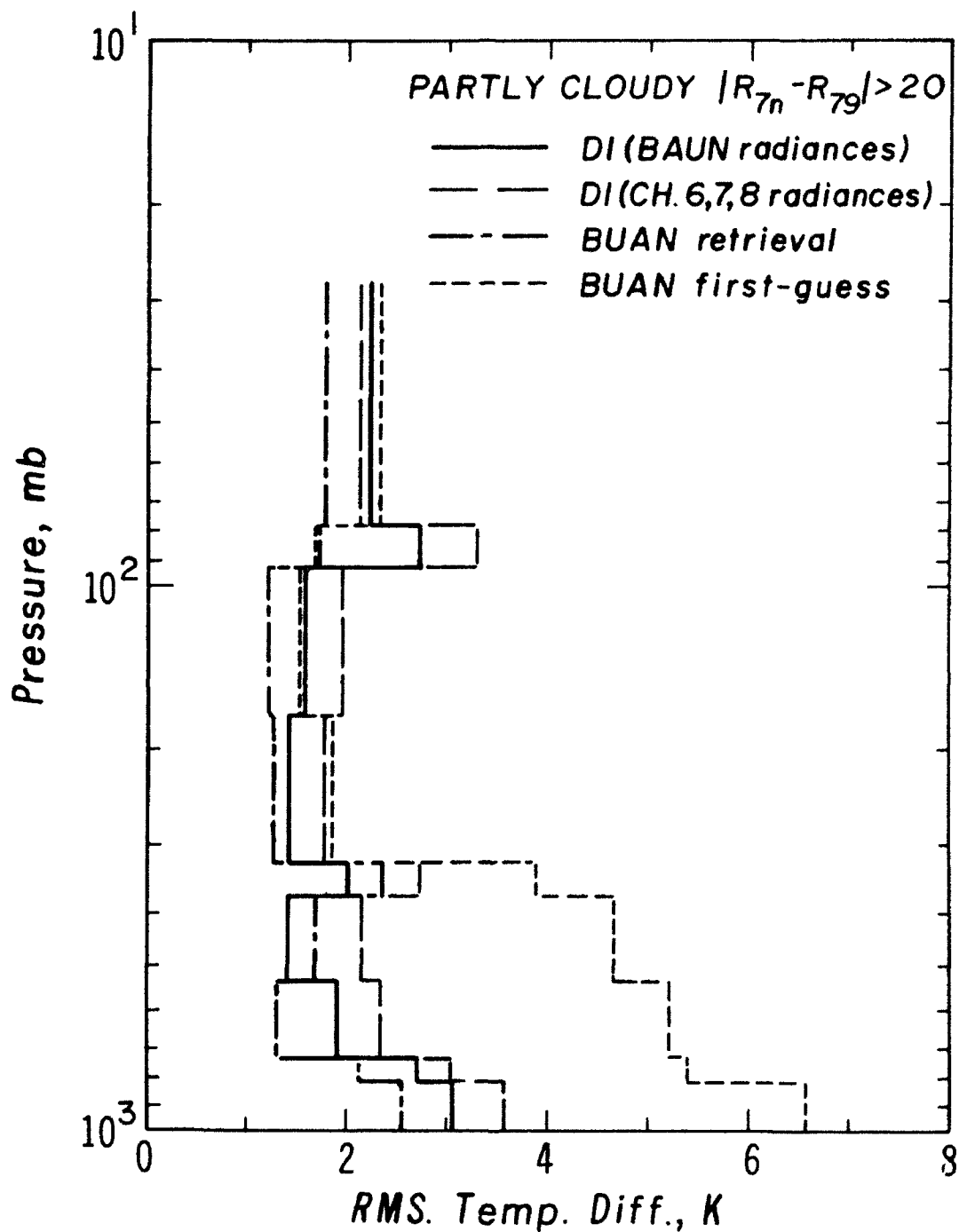
50

Fig. 12   The vertical profiles of rms temperature differences for partly-
cloudy conditions using the DI and BUAN schemes. Two sets of
radiances are used in DI; one is the cloud-removed radiances by the
current multi-spectral cloud-removal method, while the other is the
cloud-removed radiances by the BUAN N*-method.

However, the larger rms differences from the present method show that the present multi-spectral cloud-removal scheme requires further improvements. One such improvement involves the determination of the slopes G_{ij}. Additional information is required to examine how close are the cloud properties of the selected pair of spots. We may derive this information by using the collocated HIRS and AVHRR satellite data. Both HIRS and AVHRR channels are on board NOAA polar-orbiting satellites. AVHRR has five imaging channels with very high resolution (~1 km for HPRT data). Thus, one single HIRS pixel contains about 500 AVHRR pixels. From the AVHRR data, the statistics of cloud temperature and the radiative properties may be determined for each HIRS pixel. This information may be used to determine a more reliable slope G_{ij} than the adjacent-pixel method. The idea of using the collocated HIRS and AVHRR data has been proposed by Aoki (1980). This is an area requiring further research effort in connection with the present cloud removal scheme.

Between 100 and 800 mb, the rms differences for DI using the multi-spectral method are about 2 K. This performance is comparable to many other schemes (e.g., Susskind et al., 1984; Eyre, 1989). Moreover, the present multi-spectral method can be applied to cases involving both land and ocean surfaces. The operational N^*-method uses the combined 4.3 μm and microwave channels to determine N^* over the oceans. Over land, only 4.3 μm channels can be used. As a comparison, Table 5 lists the vertically averaged rms differences for both DI and BUAN schemes over land. It has been well known that temperature retrievals over land are less satisfactory due to the nonhomogeneity of surface temperature. The table shows that the vertically averaged rms differences are all larger than 2 K. Using the same BUAN radiances, the average rms difference for DI is larger than that for BUAN scheme by 0.37 K, due to the humidity effects near the surface. However, using DI, the vertically averaged rms difference using the

Table 5   Vertically averaged rms temperature differences for both DI and BUAN
            partly cloudy retrievals over land.

BUAN		DI	
first-guess	retrieved	BUAN rad.	CH678 rad.
4.95 K	2.40 K	2.77 K	2.86 K

multi-spectral radiances is only 0.09 K larger than that using the BUAN

radiances. This shows that the performance of the present multi-spectral cloud-

removal scheme is comparable to the BUAN N^*-method over land.

Section 7

CONCLUSIONS

In this report, we have presented the applicability of DI to temperature retrievals using measured satellite data. We first review the fundamentals of DI and formulate the radiative transfer equation that is appropriate for an infinite atmosphere. The convolution theory of bilateral Laplace transform is subsequently used to derive an expression for the local Planck intensity value. The Planck intensity in real space can be exactly expressed as a linear sum of the higher-order derivatives of radiance profiles. The inversion coefficient in each term of the summation can be obtained based on a generalized form of weighting functions. The higher-order derivatives of radiance profiles can be obtained by fitting the radiances for a finite number of channels using a polynomial function.

The satellite data set used in the present study contains collocated brightness temperature and radiosonde data which have been collected during the period of the BUAN experiment. The brightness temperature data include both cloud-contaminated and clear cases. Cloud-removed clear brightness temperatures obtained from the operational N^*-method are also included. The satellite data set also contains the first-guess and retrieved temperature profiles.

A new cloud removal method has been developed in conjunction with DI. This method reconstructs clear radiances from cloud-contaminated brightness temperatures using the principle of the N^*-method. The present method uses the radiances of HIRS Chs. 6, 7, and 8 to determine clear radiances and surface temperature simultaneously, based on radiative transfer simulations. In this multi-spectral method, radiance correlations for the three channels are first developed. The linear relationships between partly cloudy radiances for the two

sets of channels are subsequently used to obtain another set of clear-radiance equations. The above correlation equations are solved simultaneously using an iterative approach.

We have selected HIRS Chs. 1-7 and Chs. 13-17 to carry out temperature retrievals using DI. The large radiosonde data set along with a transmittance model are employed to compute a set of weighting function profiles. Each profile is then fitted to the generalized form to obtain the sharpness index parameters and peak pressure levels. The average values of these parameters are used in the retrievals. The strategy in determining the optimal degree of polynomial to be used in retrievals is subsequently discussed. To apply DI, which is a linear inversion method, to a nonlinear temperature retrieval problem, we have developed an adjustment scheme to derive linear radiances from satellite data. We compute a large number of linear and simulated radiances based on forward radiative transfer calculations. For each channel, a correlation in the form of quadrature fitting is established between the linear and simulated radiances. These correlations are used to convert measured radiances to simulated radiances, thus removing major nonlinear components from the data. The rms differences between the computed and fitted linear radiances are generally less than 1.3 $mW/m^2/sr/cm^{-1}$, indicating that the linear and simulated radiances are highly correlated.

Results of retrievals and their physical significance are presented and discussed. Comparisons of retrieval results using linear, simulated and BUAN radiances illustrate the effects of radiance differences due to correlations, instrument noise, collocation error, and model error. The retrieval results from DI are comparable to those from the BUAN scheme, which has rms differences between 1 - 2 K. Near the surface and tropopause, rms differences using DI are somewhat larger because the humidity effects are neglected in the retrieval. In

addition, the temperature inversion at the tropopause cannot be properly represented by polynomials. Further studies along these lines are needed. The present multi-spectral cloud-removal scheme produces retrieval accuracies that are comparable to operational schemes. Further improvements of the cloud-removal scheme will require the utilization of collocated HIRS and AVHRR data. Finally, we demonstrate that the multi-spectral cloud-removal method can be particularly useful for the determination of surface temperature over land, where the application of microwave techniques may be questionable.

REFERENCES

Abramowitz, M., and I. A. Stegun, 1972: Handbook of Mathematical Functions. Dover Publications, Inc., N.Y., 1046 pp.

Aoki, T., 1980: A statistical method to retrieve the clear radiance from cloud-contaminated radiances. J. Meteorol. Soc. Jap., 58, 524-536.

Bloom, H. J., and A. J. Nappi, 1990: The effect of a reduced sample of time and space coincident satellite/radiosonde collocations on retrieval accuracy statistics. In Preprint of the Fifth Conference on Satellite Meteorology and Oceanography, September 3-7, 1990, London, England.

Burroughs, W. J., 1991: Watching the World's Weather. Cambridge University Press, 196 pp.

Chahine, M., 1970: Inverse problems in radiative transfer: Determination of atmospheric parameters. J. Atmos. Sci., 27, 960-967.

Eyre, J. R., 1989: Inversion of cloudy satellite sounding radiances by nonlinear optimal estimation. I: Theory and simulation for TOVS. Quart. J. Roy. Meteorol. Soc., 115, 1001-1026.

Eyre, J. R., and P. D. Watts, 1987: A sequential estimation approach to cloud-clearing for satellite temperature sounding. Quart. J. Roy. Meteor. Soc., 113, 1349-1376.

Fleming, H. E., M. D. Goldberg, and D. S. Crosby, 1986: Minimum variance simultaneous retrieval of temperature and water vapor from satellite radiance measurements. Preprints, Second Conference on Satellite Meteorology/Remote Sensing and Applications (Williamsburg, Va.), Amer. Meteor. Soc., Boston, pp. 20-23.

Houghton, J. T., F. W. Taylor, and C. D. Rodgers, 1984: Remote Sounding of Atmospheres. Cambridge University Press, Cambridge, 343 p.

Kalnay, E., M. Kanamitsu, and W. E. Baker, 1990: Global numerical weather prediction at the National Meteorological Center. Bull. Amer. Meteor. Soc., 71, 1410-1428.

King, J. I. F., 1985: Theory and application of differential inversion to remote temperature sensing. In Advances in Remote Sensing Retrieval Method, H. E. Fleming and M. T. Chahine (Eds.), Deepak Publishing Co., New York, 437-444.

Liou, K. N., and S. C. Ou, 1988: Remote sounding of atmospheric temperature profiles using the differential inversion method. Report, AFGL-TR-88-0152, Air Force Geophysics Laboratory, Hanscom AFB, MA 01731, 48 pp, ADA199896.

Liou, K. N., S. C. Ou, and J. I. F. King, 1989: On the differential inversion method for temperature retrievals. In RSRM '87, Advances in Remote

Sensing Retrieval Methods, H. E. Fleming and J. S. Theon (Eds.), Deepak Publishing Co., New York, 143-156.

McCleese, D. J., and L. S. Wilson, 1976: Cloud top heights from temperature sounding instruments. Quart. J. Roy. Meteor. Soc., 102, 781-790.

McMillin, L. M., 1978: An improved technique for obtaining clear radiances from cloud-contaminated radiances. Mon. Wea. Rev., 106, 1590-1597.

McMillin, L. M., 1991: Evaluation of a classification method for retrieving atmospheric temperatures from satellite measurements. J. Appl. Meteor., 30, 432-446.

McMillin, L. M., and C. Dean, 1982: Evaluation of a new operational technique for producing clear radiances. J. Appl. Meteor., 21, 1005-1014.

McMillin, L. M., H. E. Fleming, and M. L. Hill, 1979: Atmospheric transmittance of an absorbing gas. 3: A computationally fast and accurate transmittance model for absorbing gases with variable mixing ratios. Appl. Optics, 18, 1600-1606.

Ou, S. C., and K. N. Liou, 1989: Remote sounding of atmospheric temperature profiles using the optical measure method. Report, AFGL-TR-89-0346, Air Force Geophysics Laboratory, Hanscom AFB, MA 01731, 64 pp, ADA244828.

Pearson, C. E., 1974: Handbook of Applied Mathematics. Van Nostrand Reinhold Co., New York, 87-89.

Phillips, N., J. Susskind, and L. M. McMillin, 1988: Results of a joint NOAA/NASA sounder simulation study. J. Atmos. Ocean. Tech., 5, 44-56.

Reale, A. L., D. G. Gray, A. Swaroop, and A. Nappi, 1986: Higher resolution operational satellite retrievals. In Preprint of the 2nd Conference on Satellite Meteorology/Remote Sensing and Applications, May 13-16, 1986, Williamsburg, Va.

Smith, W. L., 1968: An improved method for calculating tropospheric temperature and moisture from satellite radiometer measurements. Mon. Wea. Rev., 96, 387-396.

Smith, W. L., and H. M. Woolf, 1976: The use of eigenvectors of statistical covariance matrices for interpreting satellite sounding radiometer observations. J. Atmos. Sci., 33, 1127-1150.

Smith, W. L., H. M. Woolf, C. M. Hayden, D. Q. Wark, and L. M. McMillin, 1979: The TIROS-N Operational Vertical Sounder. Bull. Amer. Meteor. Soc., 60, 1177-1187.

Smith, W. L., H. L. Huang, S. A. Ackerman, and H. E. Revercomb, 1990: Sounding through semi-transparent cloud with high resolution infrared radiance spectra. In Preprint of the 5th Conference on Satellite Meteorology and Oceanography, September 3-7, 1990, London, England.

Susskind, J., J. Rosenfield, and D. Reuter, 1983: An accurate radiative transfer model for use in the direct physical inversion of HIRS2 and MSU temperature sounding data. J. Geophy. Res., 88, 8550-8568.

Susskind, J., J. Rosenfield, and D. Reuter, 1984: Remote sensing of weather and climate parameters from HIRS/MSU on TIROS-N. J. Geophy. Res.., 89, 4677-4697.

Widder, D. V., 1971: An Introduction to Transform Theory. Academic Press, New York, 253 pp.

Appendix

BUAN RETRIEVAL PROCEDURES

Starting with the 9x7 array, numerous clear tests are performed on each of the 63 spots to search for clear spots. Those spots which pass all the clear tests are defined as clear. The rest of the spots are subject to cloud-removal process using the N^* method (McMillin, 1978). Certain restrictions are applied in the usage of the N^* method. Those spots in which the N^* method is applicable are defined as partly cloudy. The remaining spots are defined as cloudy.

The 63 spots are further divided into six miniboxes, each of which contains an array of 3 x 3 spots (dashed frames in Fig. 3.1). A minibox has a footprint of 50 km at the nadir. For each minibox, the radiance sets for the nine spots are examined. If one or more spots have been declared clear, then the minibox is defined as clear. Only one set of clear radiances is produced for each minibox. If only one spot is found to be clear in the minibox, the radiances of this spot are selected to be the representative clear radiances of the minibox. If more than one spot in the minibox is declared to be clear, these spots are subject to a test to determine the spot that is the "clearest." This test involves comparison between predicted and observed MSU channel radiances. The predicted MSU channel radiances are obtained by an interchannel regression equation. The spot that shows the least difference between predicted and observed MSU radiances is flagged as the "clearest."

If only partly cloudy spots are contained in the minibox, the minibox is defined as cloudy. Again, only one set of cloud-removed clear radiances is to be produced to represent the minibox. For this purpose, the radiances of all partly-cloudy spots are subject to tests to determine the "best" cloud-removed clear radiances. These tests include the interchannel regression test that is

60

performed to determine the "clearest" spot, and the search for the most successful N* correction. The radiances for the "best" partly cloudy spot are selected for the partly-cloudy minibox.

If none of the spots in the minibox are either clear or partly cloudy, the minibox is defined as cloudy. In this case, the spot with the highest value of Ch. 7 radiances is selected. The representative "clear" radiances for a cloudy minibox are the average of all radiances of the nine adjacent spots.

For each box, there are six sets of representative clear radiances, representing a tremendous amount of data volume. Further filtering tests are then performed to reduce the data volume. Each minibox is flagged to be "good," "redundant," "questionable" or "bad." Thus only those miniboxes which are flagged "good" are used in the subsequent retrieval analyses.

To retrieve atmospheric temperature profiles, the TOVS operational retrieval algorithm is used. This program uses a minimum-variance simultaneous retrieval technique (Fleming et al., 1986). Theories of the minimum variance method have been described by Houghton et al. (1984). The main part of this retrieval algorithm is to solve the following matrix equation:

$$\Delta \vec{x} = CK^T (KCK^T + E)^{-1} \Delta \vec{y}, \qquad (A.1)$$

where $\Delta \vec{x}$ denotes the difference between the final solution and the first-guess solution vectors, C is the expected error covariance matrix for the first-guess vector, K is the kernel matrix $(\partial y_i / \partial x_j)$, of which the elements can be derived from the radiative transfer equation, E is the expected error covariance matrix of the combined measurement and forward radiative transfer model errors, and $\Delta \vec{y}$ is the difference between the observed and model-generated radiances.

Determination of the first-guess profile is an important step in the minimum-variance method because the final solution strongly depends on it.

Procedures to compute the first-guess vector are based on a sample of previously collocated radiosonde and satellite observations. Twenty sets of radiances among a 28-day data set collected prior to the observation date are selected. They are closest to the observed radiance vector for a given sounding. The selected radiances are averaged to derive the initial estimates of first-guess radiances for the retrieval. The twenty associated temperature and moisture profiles derived from the statistical regression equation are also averaged to produce the first-guess solution vectors. The 28-day data set is categorized according to latitude, land/sea and day/night flags, and is updated each week.